NUSC Technical Report 5391

NUSC Technical Report 5391

Propagation Loss Model Assessment at Low Frequencies in a Bottom-Limited Region

Grant Gartrell
Frederick R. DiNapoli
Ocean Sciences & Technology Department

30 June 1976

NUSC

NAVAL UNDERWATER SYSTEMS CENTER
Newport, Rhode Island • New London, Connecticut

PREFACE

The experimental data were obtained and processed in conjunction with NUSC Project No. A65408, Subproject ZR 000-01-01, "BILL (Below and In Layer Propagation Loss Studies)," Principal Investigator, Dr. F. R. DiNapoli (Code TA113), and the sponsoring activity is Naval Material Command (CNM/DLP/MAT 03L4, Dr. J. H. Huth). The analysis and preparation of this report were funded by NUSC Project No. A65002, Subproject No. SF 52-522-701, Principal Investigator, Dr. F. R. DiNapoli (Code TA113). The sponsoring activity is Naval Sea Systems Command (SEA—06H1-4), Program Manager, A. P. Franceschetti.

Dr. Grant Gartrell has participated in this study under the auspices of the Mutual Weapons Development Data Exchange Agreement N-74-A-5815 (Underwater Acoustics Research) Marvin A. Blizzard, U.S. Project Officer (ONR Code 212).

The Technical Reviewer for this report was J. S. Cohen (Code PA41).

REVIEWED AND APPROVED: 30 June 1976

R. W. Hasse
Associate Director for Sonar Research

G. Gartrell is located at the Weapons Research Establishment, Salisbury, South Australia.

F. R. DiNapoli is located at the New London Laboratory, Naval Underwater Systems Center, New London, Connecticut 06320.

REPORT DOCUMENTATION PAGE

READ INSTRUCTIONS BEFORE COMPLETING FORM

REPORT NUMBER: NUSC-TR-5391	2. GOVT ACCESSION NO.
3. RECIPIENT'S CATALOG NUMBER: Technical Rept.	
4. TITLE (and Subtitle): PROPAGATION LOSS MODEL ASSESSMENT AT LOW FREQUENCIES IN A BOTTOM-LIMITED REGION,	5. TYPE OF REPORT & PERIOD COVERED
	6. PERFORMING ORG. REPORT NUMBER
7. AUTHOR(s): Grant Gartrell Frederick R. DiNapoli	8. CONTRACT OR GRANT NUMBER(s)
9. PERFORMING ORGANIZATION NAME AND ADDRESS Naval Underwater Systems Center New London Laboratory New London, CT 06320	10. PROGRAM ELEMENT, PROJECT, TASK AREA & WORK UNIT NUMBERS A65002 SF 52-522-701
11. CONTROLLING OFFICE NAME AND ADDRESS Naval Sea Systems Command (SEA 06H1-4) Washington, DC 20362	12. REPORT DATE: 30 June 1976
	13. NUMBER OF PAGES: 50
14. MONITORING AGENCY NAME & ADDRESS (if different from Controlling Office): NUSC-11-650-02; SF52-522	15. SECURITY CLASS. (of this report): UNCLASSIFIED
	15a. DECLASSIFICATION/DOWNGRADING SCHEDULE

16. DISTRIBUTION STATEMENT (of this Report)

Approved for public release; distribution unlimited

SF52-522-701

17. DISTRIBUTION STATEMENT (of the abstract entered in Block 20, if different from Report)

18. SUPPLEMENTARY NOTES

19. KEY WORDS (Continue on reverse side if necessary and identify by block number)

Propagation Loss Models
Bottom-Limited Regions
Bottom Modeling

20. ABSTRACT (Continue on reverse side if necessary and identify by block number)

A physical insight into the problem of low frequency propagation loss modeling in a bottom-limited region is gained by comparison of a representative range of prediction models with a precisely determined set of experimental data. One series of the Project BILL (Below and In Layer Propagation Loss) measurements was conducted at 100 Hz during December 1973 in the Tongue of the Ocean, Bahama Islands, at a water depth of approximately 1800 meters.

DD FORM 1 JAN 73 1473

405918

20. (Cont'd)

A pulsed CW acoustic projector was towed at a depth of 76 meters along an accurately determined track to a range of 40 kiloyards. The pulses were received at hydrophones located both in and below the surface duct. Despite excellent experimental control, predictions from various propagation loss models have been unable to reproduce major features of the multipath interference structure of the data. Although few firm conclusions are possible, the report discusses several possible contributory causes for the discrepancies, major among these being inadequate bottom modeling. Implications for future trends in the development of low frequency propagation loss models for bottom-limited regions are briefly examined.

TABLE OF CONTENTS

	Page
LIST OF TABLES	ii
LIST OF ILLUSTRATIONS	ii
INTRODUCTION	1
EXPERIMENTAL DATA	2
BASIS AND OBJECTIVES FOR MODEL ASSESSMENT	4
RANGE-INDEPENDENT CW MODEL COMPARISONS	17
EFFECT OF FINITE PULSE LENGTH	25
BOTTOM MODELING	25
Phase Path Geometry	25
Kanabis Shallow Water Model	27
Three-Dimensional Bottom Topography	30
SUBBOTTOM MODELING	32
AN OBSTACLE TO RANGE-DEPENDENT PULSE MODELING	37
CONCLUSIONS	42
REFERENCES	44

LIST OF TABLES

Table		Page
1	Acoustic Propagation Loss Models Employed In This Study	2
2	Station 3 Sound-Speed Profile Extended to Maximum Depth of 1828.8 m (1000 fm)	19

LIST OF ILLUSTRATIONS

Figure		Page
1	Environmental Data	3
2	Total Energy Propagation Loss (Receiver Depth, 15 m)	5
3	Total Energy Propagation Loss (Receiver Depth, 76 m)	6
4	Total Energy Propagation Loss (Receiver Depth, 107 m)	7
5	Total Energy Propagation Loss (Receiver Depth, 229 m)	8
6	Total Energy Propagation Loss (Receiver Depth, 350 m)	9
7	Peak Propagation Loss (Receiver Depth, 15 m)	10
8	Peak Propagation Loss (Receiver Depth, 76 m)	11
9	Peak Propagation Loss (Receiver Depth, 107 m)	12
10	Peak Propagation Loss (Receiver Depth, 229 m)	13
11	Peak Propagation Loss (Receiver Depth, 350 m)	14
12	Ray Diagram for Near-Source Region (Source Depth 76 m)	15
13	Received Signal Time Structure at Several Ranges	16
14	FFP Predictions, Source 76 m	18
15	Direct-Path Region Fit of FFP to Experimental Data (Source 76 m, Receiver 107 m), Showing Effect of Choice of Sound-Speed Profile	20
16	Perturbations to Input Parameters Establish Sensitivity Of Model Predictions to Small Errors in Placement Of Receivers.	22
17	Perturbations to Input Parameters Establish Sensitivity of Model Predictions to Small-Range or Time-Dependent Variations of Model Geometry	23
18	Effect of Finite Pulse Length on Multipath Interference Structure (Source 76 m, Receiver 107 m)	24
19	Bottom Loss Model Used for FFP Predictions.	26

LIST OF ILLUSTRATIONS (Cont'd)

Figure		Page
20	Ray Diagrams Comparing Sound Field	28
21	Range-Dependent Normal Mode (Kanabis Model) With Partial Mode Conversion (Source 76 m, Receiver 107 m)	29
22	Comparison of Horizontal Ray Theory and FFP Predictions For a Range-Independent Case (Source 76 m, Receiver 107 m)	31
23	Comparison of Horizontal Ray Theory (3-Dimensional Mode) With Experimental Data, Assuming Range-Dependent Bottom (Source 76 m, Receiver 107 m)	33
24	Parabolic Equation (Canadian) Range-Depth Propagation Loss Diagrams (Intensity Scale: White $\leq$ 60 dB; Black $\geq$ 100 dB)	35
25	Parabolic Equation (Canadian) Predictions Compared With Experimental Data (Source 76 m, Receiver 107 m)	36
26	NUSC Parabolic Equation Model Predictions for Range-Independent Case (1 m/sec/m Sound-Speed Gradient In Bottom, 0.1 dB/λ Bottom Attenuation)	38
27	NUSC Parabolic Equation Model Predictions for Range-Independent Case (4 m/sec/m Sound-Speed Gradient In Bottom, 0.01 dB/λ Bottom Attenuation)	39
28	NUSC Parabolic Equation Model Predictions for 12-Segment Range-Dependent Bottom, Otherwise Conditions Are As in Figure 27	40
29	Comparison of FFP Fourier Synthesis Pulse Propagation Loss Modeling With CONGRATS Ray Theory Model and Experimental Data (50 msec Pulse, Receiver Depth 350 m)	41

REVERSE BLANK

PROPAGATION LOSS MODEL ASSESSMENT AT LOW FREQUENCIES IN A BOTTOM-LIMITED REGION

INTRODUCTION

The importance of reliable low frequency acoustic propagation models for bottom-limited and, in particular, near-coastal regions is clearly apparent. All models invariably approximate the real situation by a simplified description, where the simplification may be brought about to accommodate lack of data or limited computing power, or perhaps as a consequence of the need for restricting models to mathematically tractable expressions. Speed of computation may also be a consideration.

Most models, whether based on ray or wave theory, assume infinite CW propagation and involve considerable extension to handle transient signals. On the other hand, most propagation loss experiments use pulsed CW or explosive sources, so that model validation itself may present problems.

Some ray theory models may be applied to situations with quite complex range dependence, but may not be appropriate at very low frequencies. Wave theory models, on the other hand, may work most efficiently at low frequencies but may be limited in ability to deal with range-dependent geometries. No single universally applicable model so far exists.

Although it is undoubtedly possible to seek out ocean regions with properties that fit an acoustic model, the converse is not necessarily true. When a situation arises for which no currently available model is ideally suited, it is often unclear as to whether predictions from one of the more sophisticated available models will be any more appropriate than those from a simpler model, since both are approximate anyway. As always, the acid test is not comparison of one model with another, but comparison of model prediction with experimental measurements.

In this study, we address the pertinent but geometrically awkward problem of modeling low frequency propagation loss in a bottom-limited region. Following a description of an experimental measurement trial, propagation loss predictions for a number of models are presented and discussed. Analysis of the shortcomings of the various prediction approaches in this application provides

a valuable physical insight into the modeling problem. Finally, a brief examination is made of the implications of the results for future trends in the development of low frequency propagation loss models for bottom-limited regions.

Models available to the authors which have been used to approach the problem from a variety of directions are listed in table 1.

Table 1. Acoustic Propagation Loss Models Employed in This Study

Fast Field Program (FFP)[1]
Ray theory with correction (NISSM II)[2]
Ray theory CONGRATS coherent addition[3]
Ray theory CONGRATS range dependent[4]
Range dependent normal mode program[5]
Horizontal ray theory[6]
Parabolic equation (P. E.) model (Canadian Version)[7]
Parabolic equation (P. E.) model (NUSC Version)[8]

EXPERIMENTAL DATA

A propagation loss measurement trial was conducted in the Tongue of the Ocean, Bahamas, on 3 December 1973. The venue lies in the AUTEC acoustic range operated by the Naval Underwater Systems Center, enabling ship positions to be accurately determined at all times by shore-based radar. The bottom topography of the region has been surveyed in detail and extensive oceanographic studies made.[9] Along the trial track, the bottom consists of mud and sand believed to thinly overlay coralline limestone. Water depth is of the order of 1500 to 1800 meters.

Signals were received on five hydrophones at depths of 15, 76, 107, 229, and 350 m below the surface at station 1 of figure 1. The source was a J15 projector, suspended at a depth of 76 m, and towed at 2 knots away from the receivers along the track shown in figure 1 to station 3, a distance of 36.5 km. The signal consisted of 100 Hz sinusoidal pulses, 50 msec in duration, at the rate of one every four seconds.

Sound velocimeter and expendable bathythermograph (XBT) casts were conducted at stations 1 and 3, with an additional midpoint XBT at station 2.

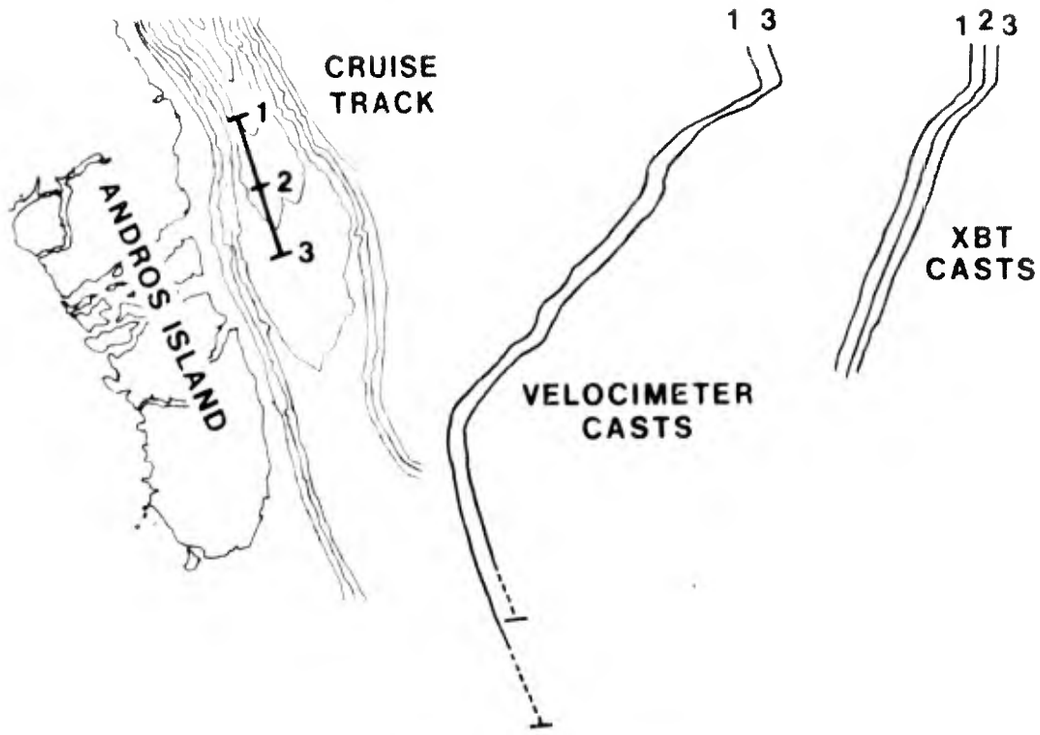

Figure 1. Environmental Data

The consistency of these measurements implies that it is not unreasonable to regard them as representative of the profiles pertaining to all points along the intermediate track. Note that the velocimeter and XBT curves have been offset for presentation in figure 1, since they are nearly indistinguishable.

Hydrophone outputs were recorded in analog form. Digital records for computer analysis were created from the original data with a sampling frequency of 512 Hz.

Propagation loss measurements were determined from these data in two ways. Figures 2 through 6 show total energy propagation loss, which takes into account all multipath arrivals which arrive within the four-second period between pulses. Figures 7 through 11 give the peak value propagation loss, determined from the strongest arrival within the four-second period.

BASIS AND OBJECTIVES FOR MODEL ASSESSMENT

The task we have set ourselves in this exercise is to attempt to replicate the data, at least to the point of matching the major features of the multipath interference structure. At higher frequencies this might be unrealistic, but at 100 Hz, perhaps not. The question of whether the goal is realistic or not bears directly on our approaches toward future model development.

Figure 12 shows a ray diagram for the near-source region of the sound field. Rays are spaced 1° apart between limits of +25° and -25°. At a frequency of 100 Hz, the surface duct will be leaky, and in 1800 m of water is not a significant factor for low bottom loss conditions.

Figure 13 shows typical received signals as a function of time at several ranges. Close to the source, the duration of the dominant arrival indicates that the overlap of the direct and surface-reflected arrivals is almost complete. Close agreement would thus be expected between total energy and peak level propagation loss determinations, and infinite CW predictions.

As range increases, particularly once all paths include bottom interactions, the arrival structure becomes more spread in time. As the number of peaks in the arrival structure increases, the probability of an individual peak containing most of the energy decreases. The peak level propagation loss determination thus tends to show generally greater loss than that for the total energy, which should agree more closely with the infinite CW predictions, disregarding the rapid fluctuations of the latter due to continuing multipath interference.

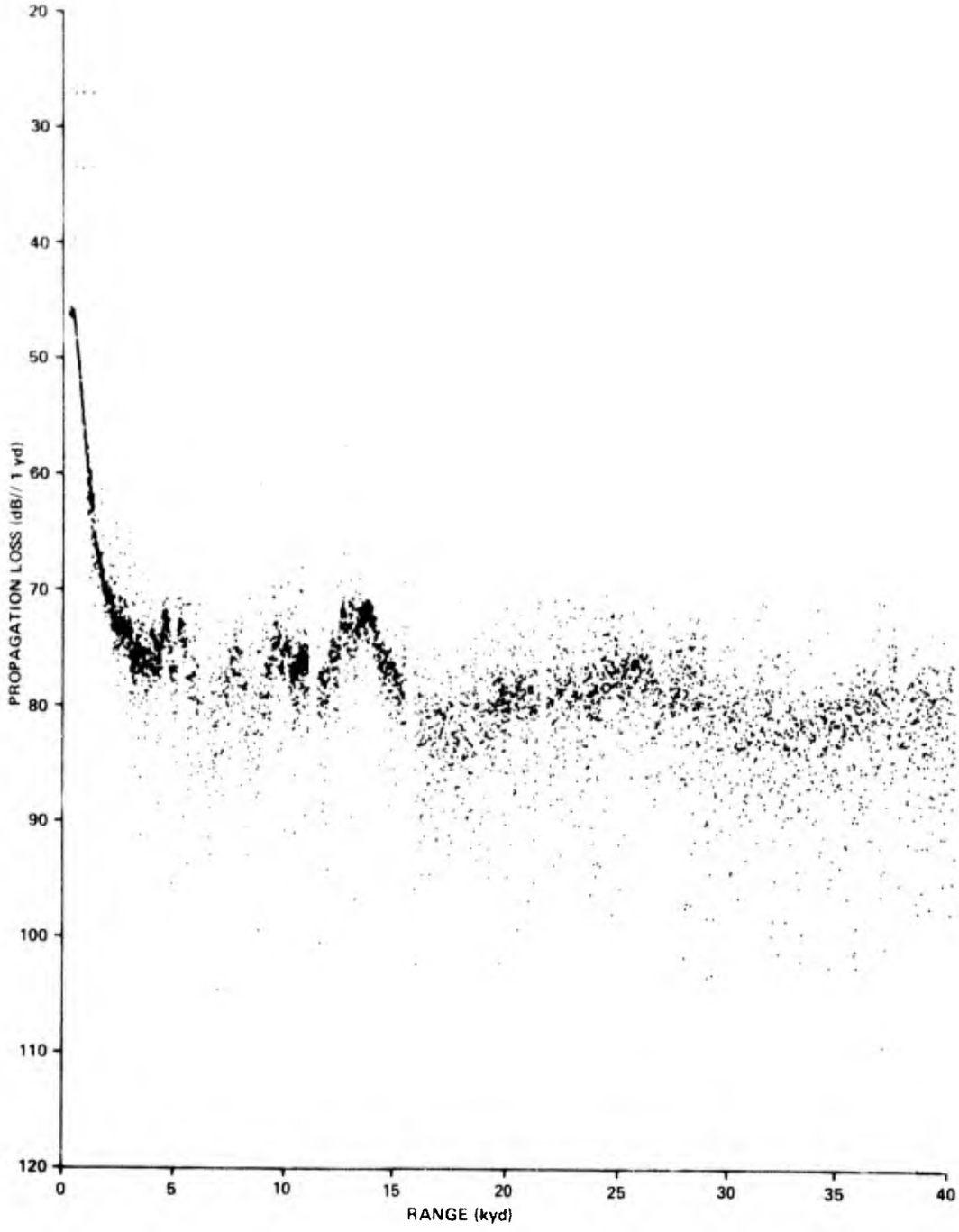

Figure 2. Total Energy Propagation Loss (Receiver Depth, 15 m)

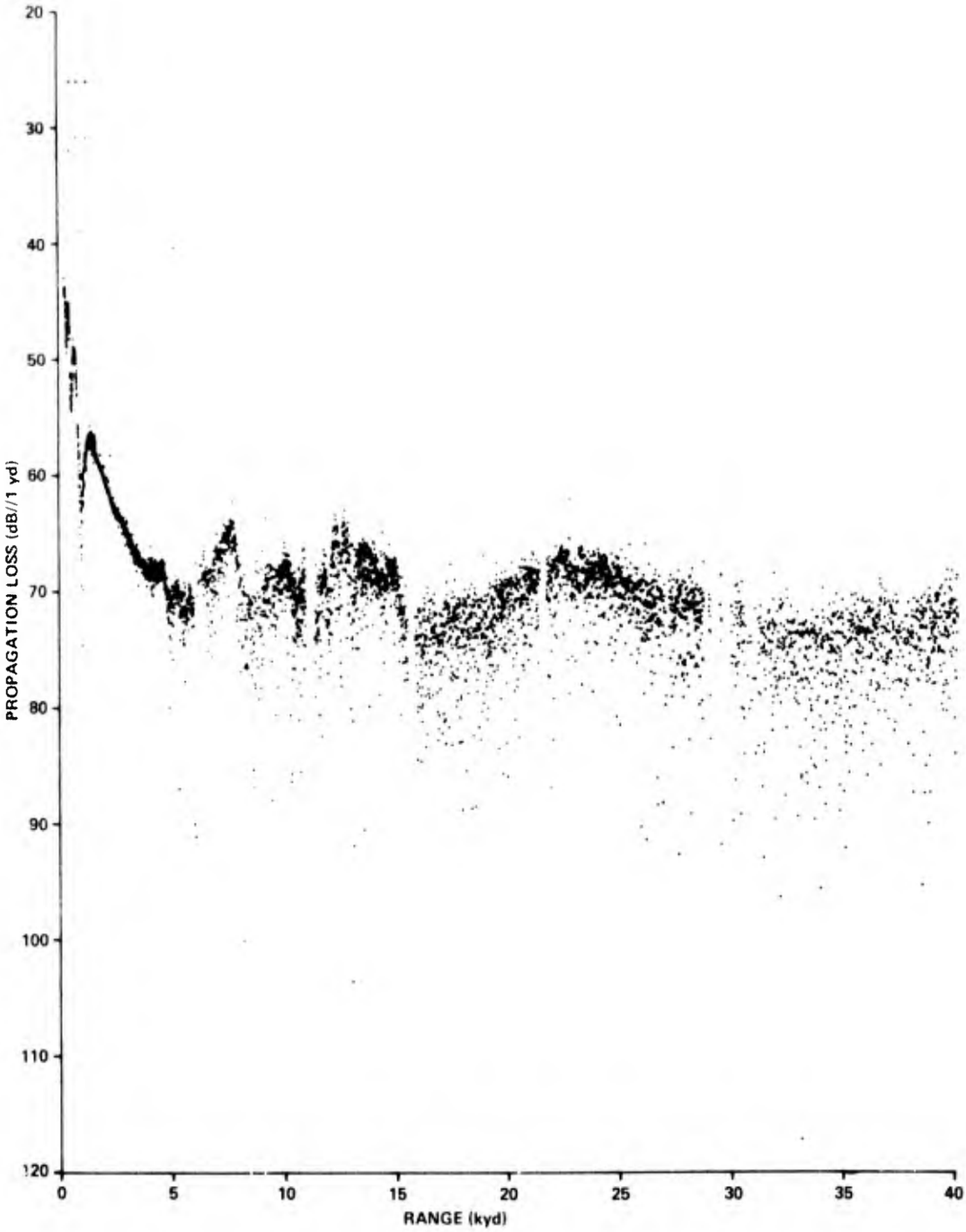

Figure 3. Total Energy Propagation Loss (Receiver Depth, 76 m)

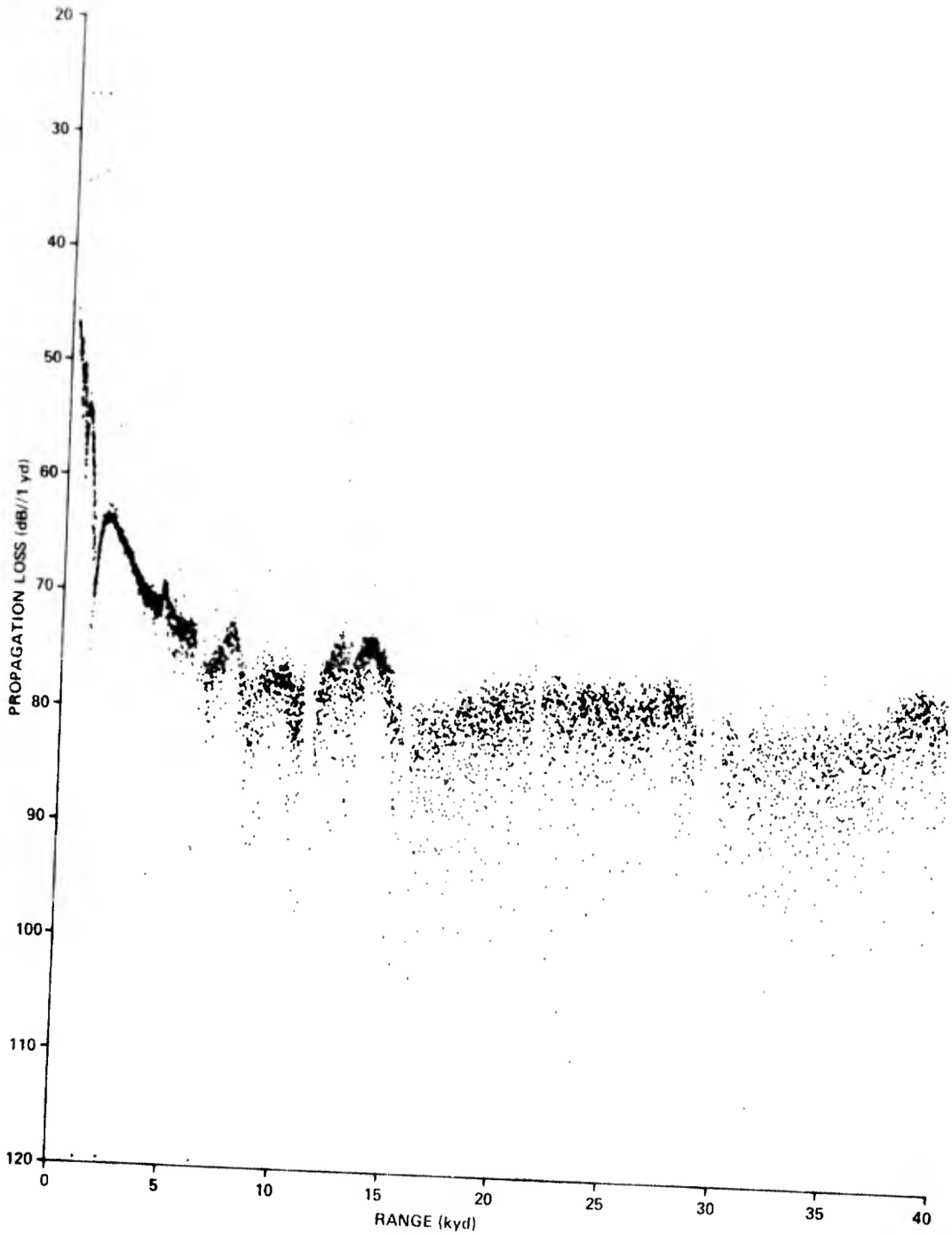

Figure 4. Total Energy Propagation Loss (Receiver Depth, 107 m)

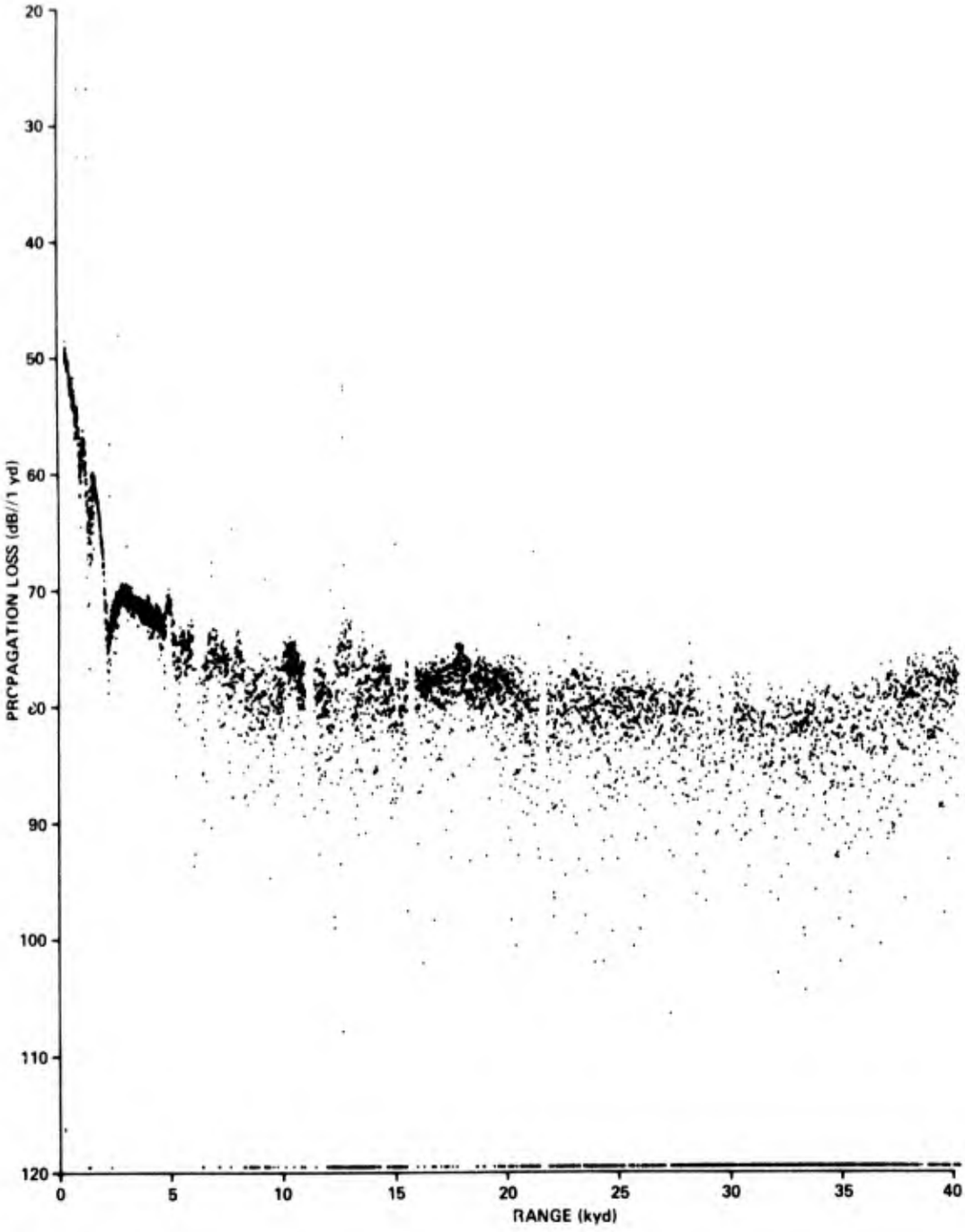

Figure 5. Total Energy Propagation Loss (Receiver Depth, 229 m)

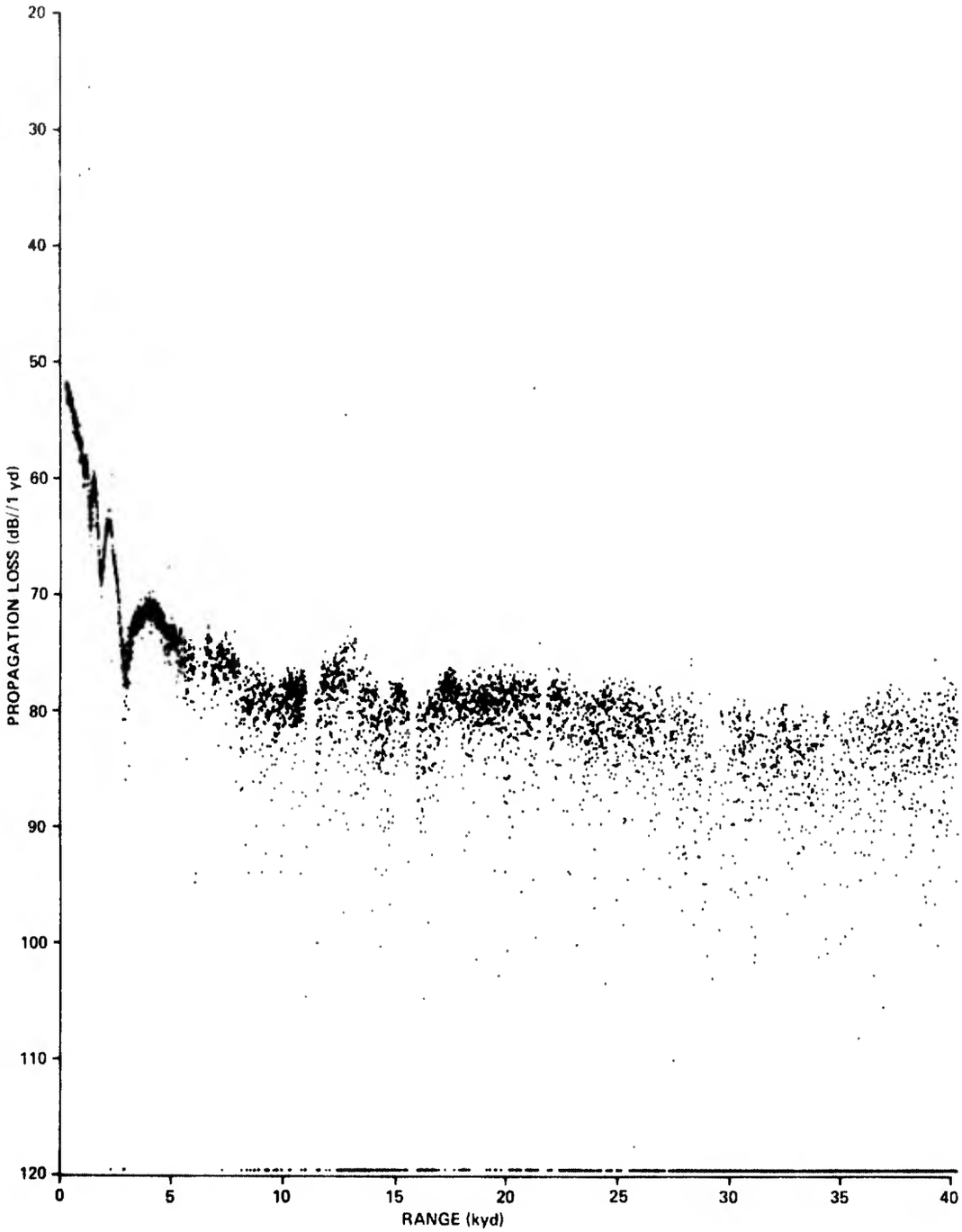

Figure 6. Total Energy Propagation Loss (Receiver Depth, 350 m)

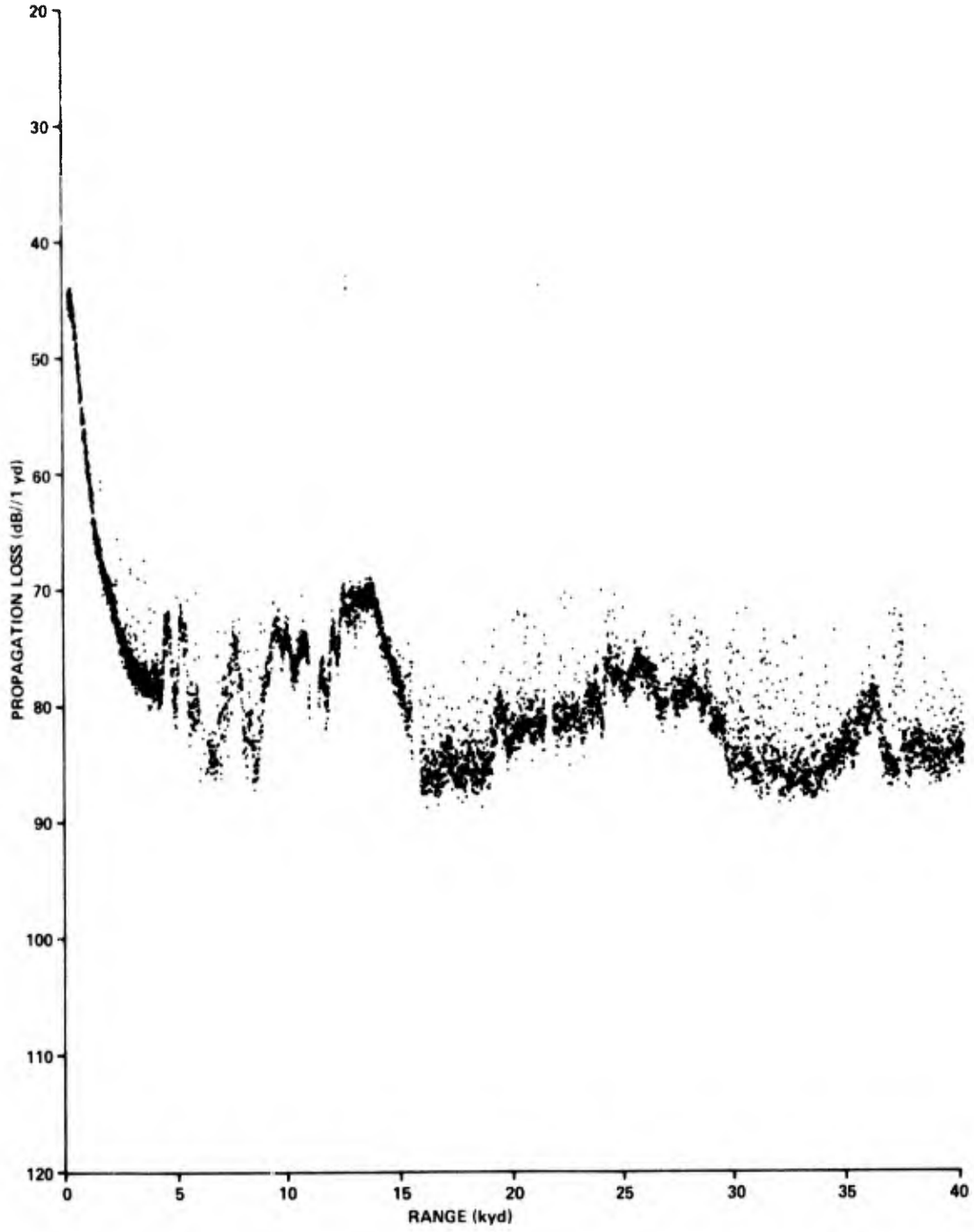

Figure 7. Peak Propagation Loss (Receiver Depth, 15 m)

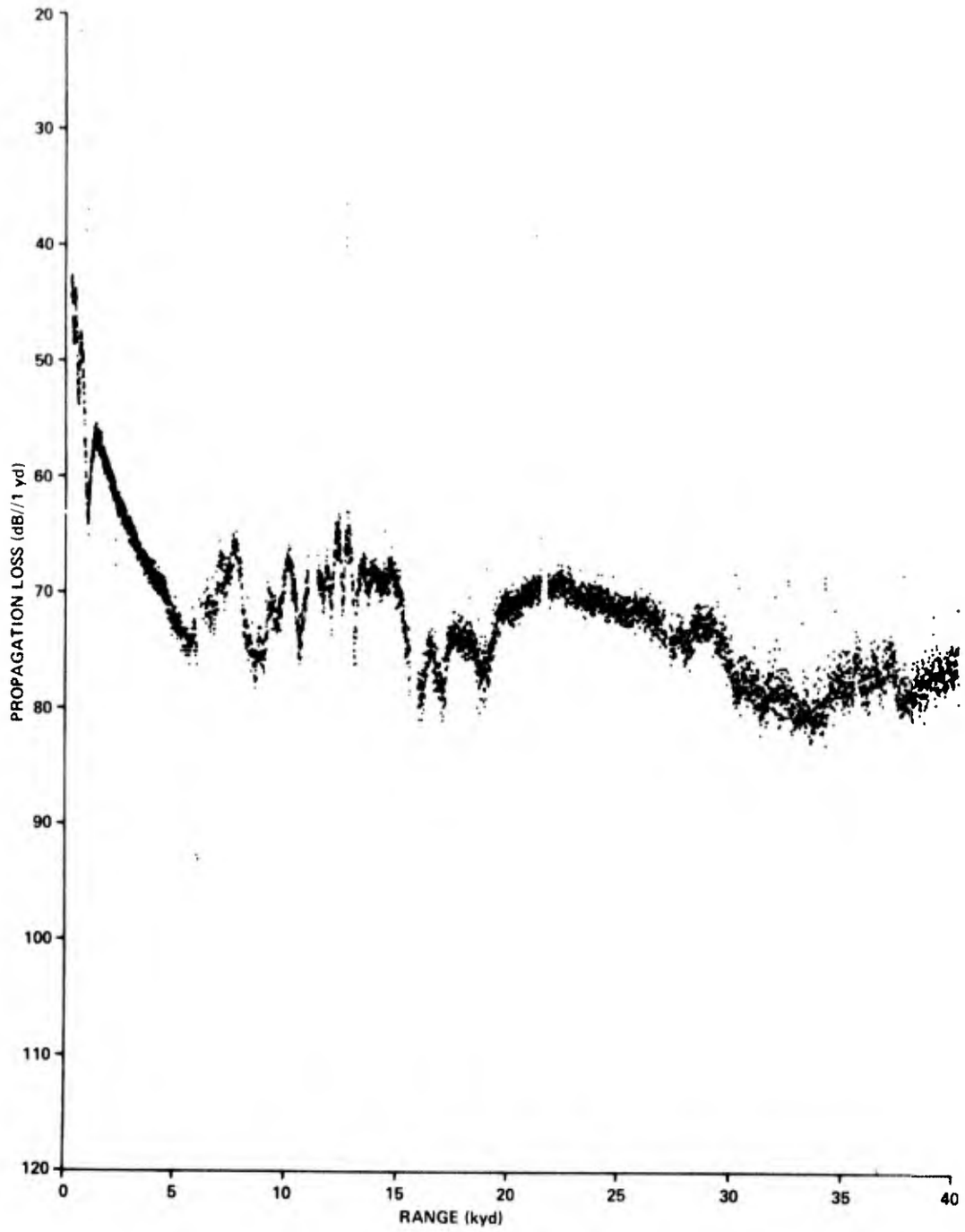

Figure 8. Peak Propagation Loss (Receiver Depth, 76 m)

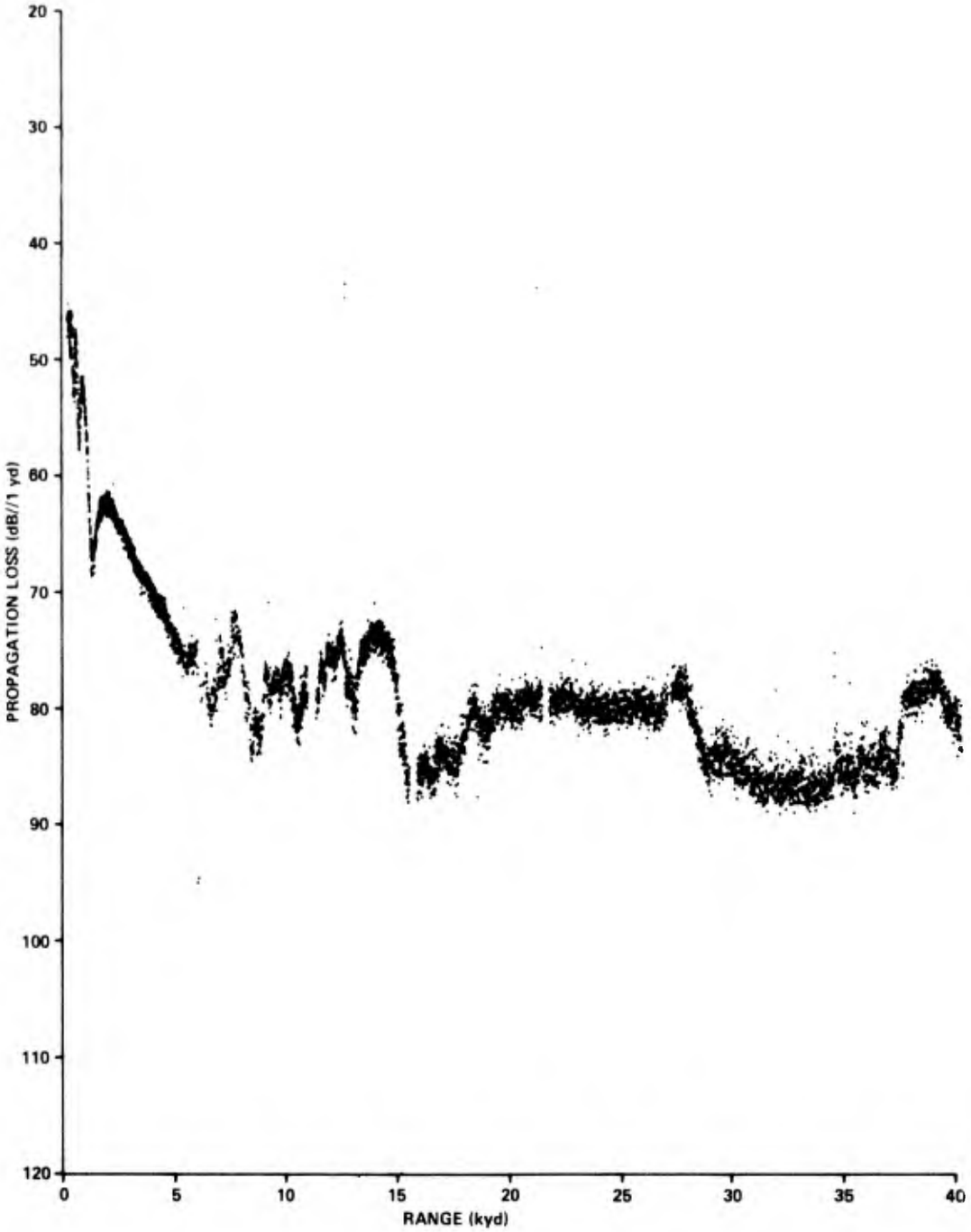

Figure 9. Peak Propagation Loss (Receiver Depth, 107 m)

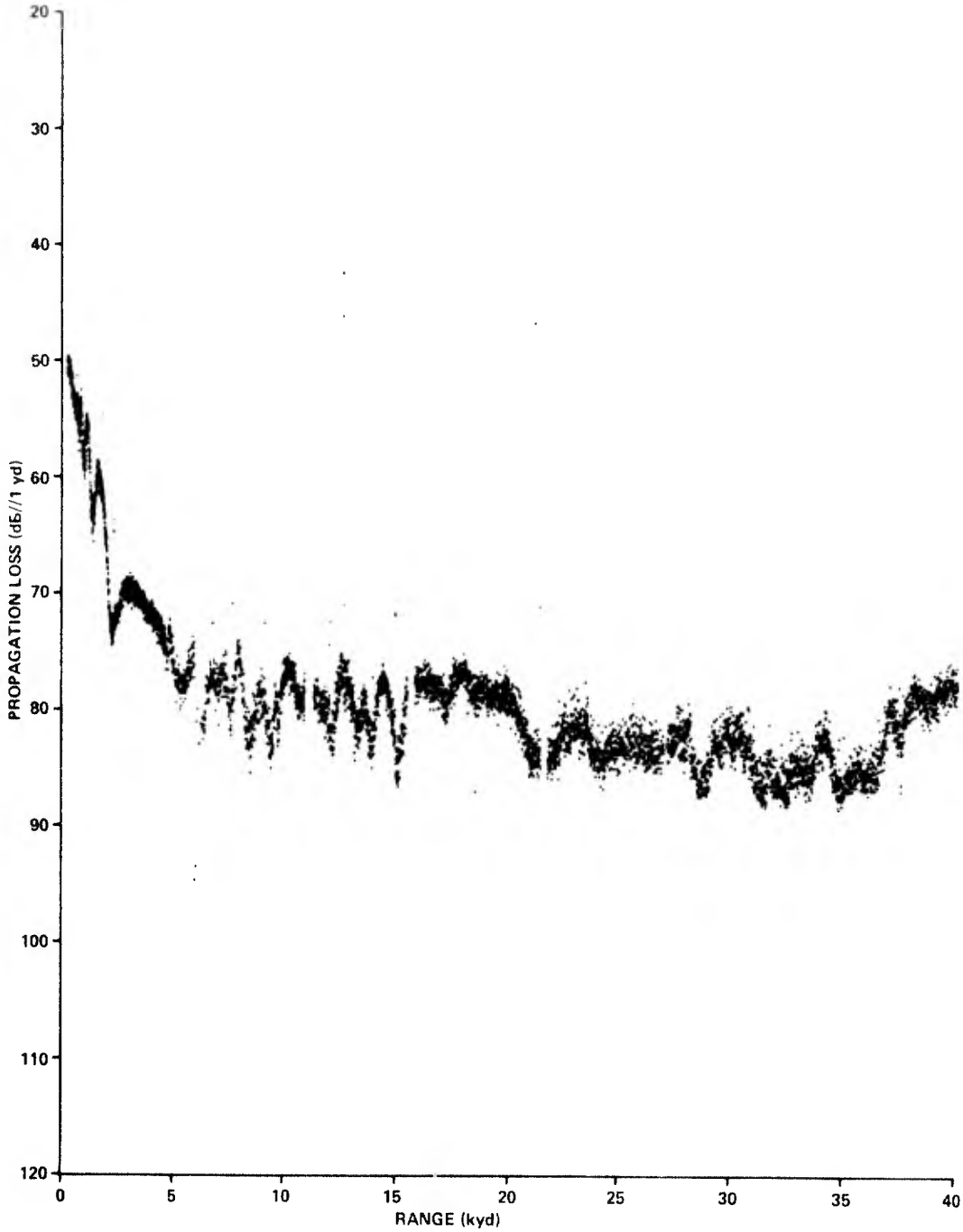

Figure 10. Peak Propagation Loss (Receiver Depth, 229 m)

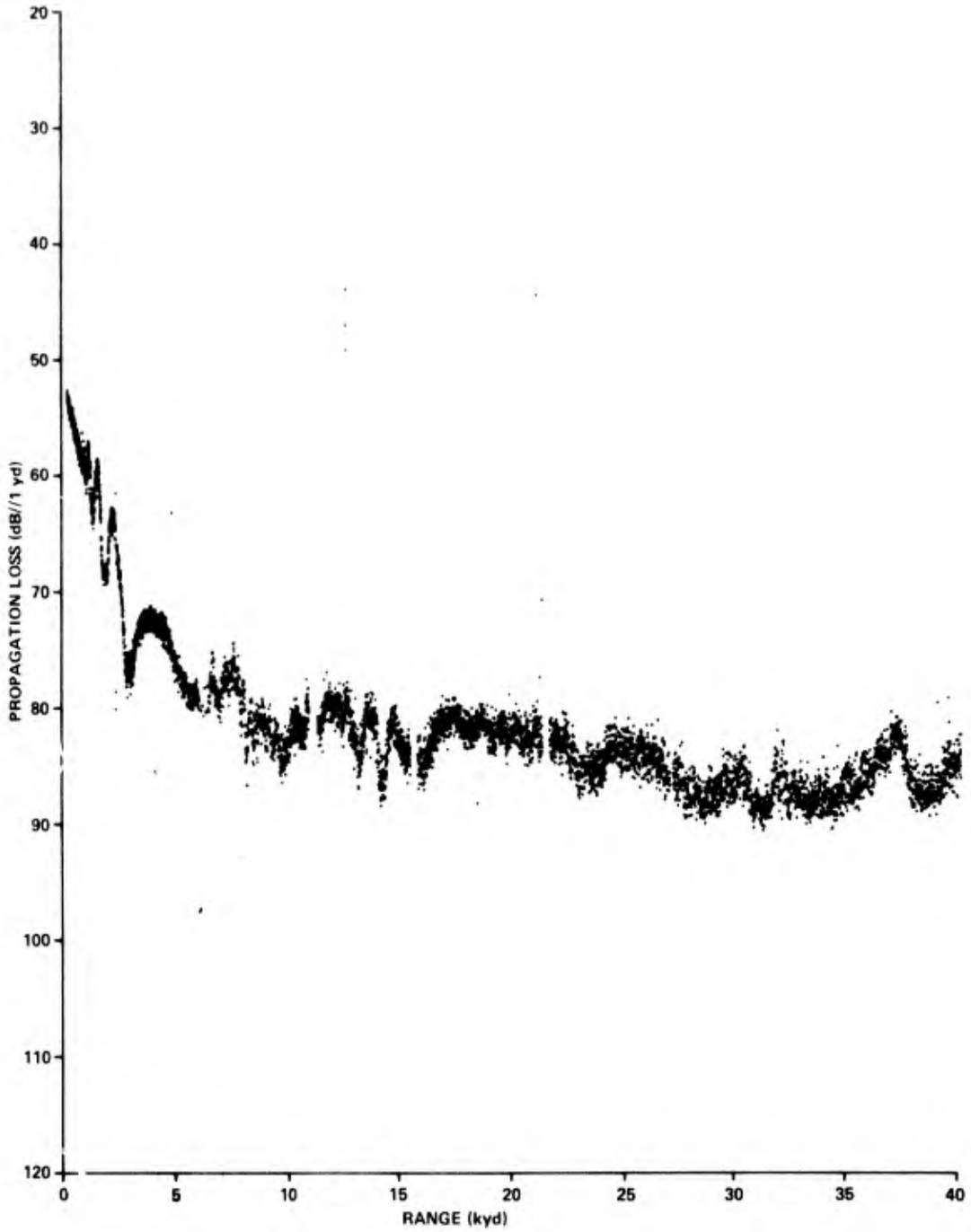

Figure 11. Peak Propagation Loss (Receiver Depth, 350 m)

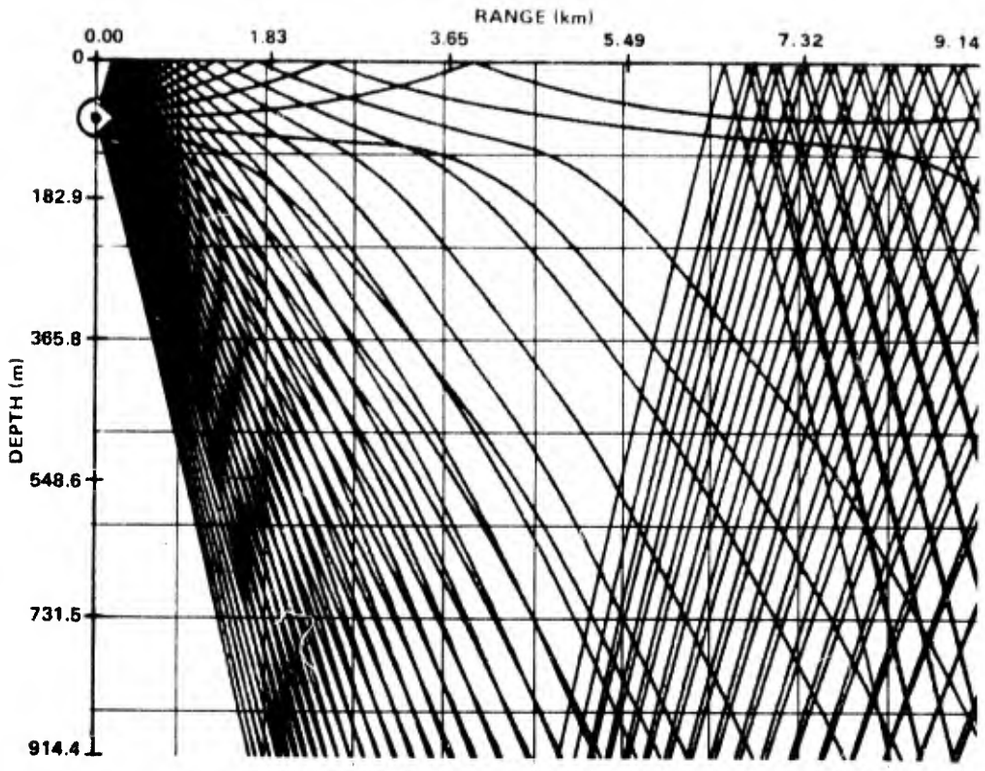

Figure 12. Ray Diagram for Near-Source Region (Source Depth 76 m)

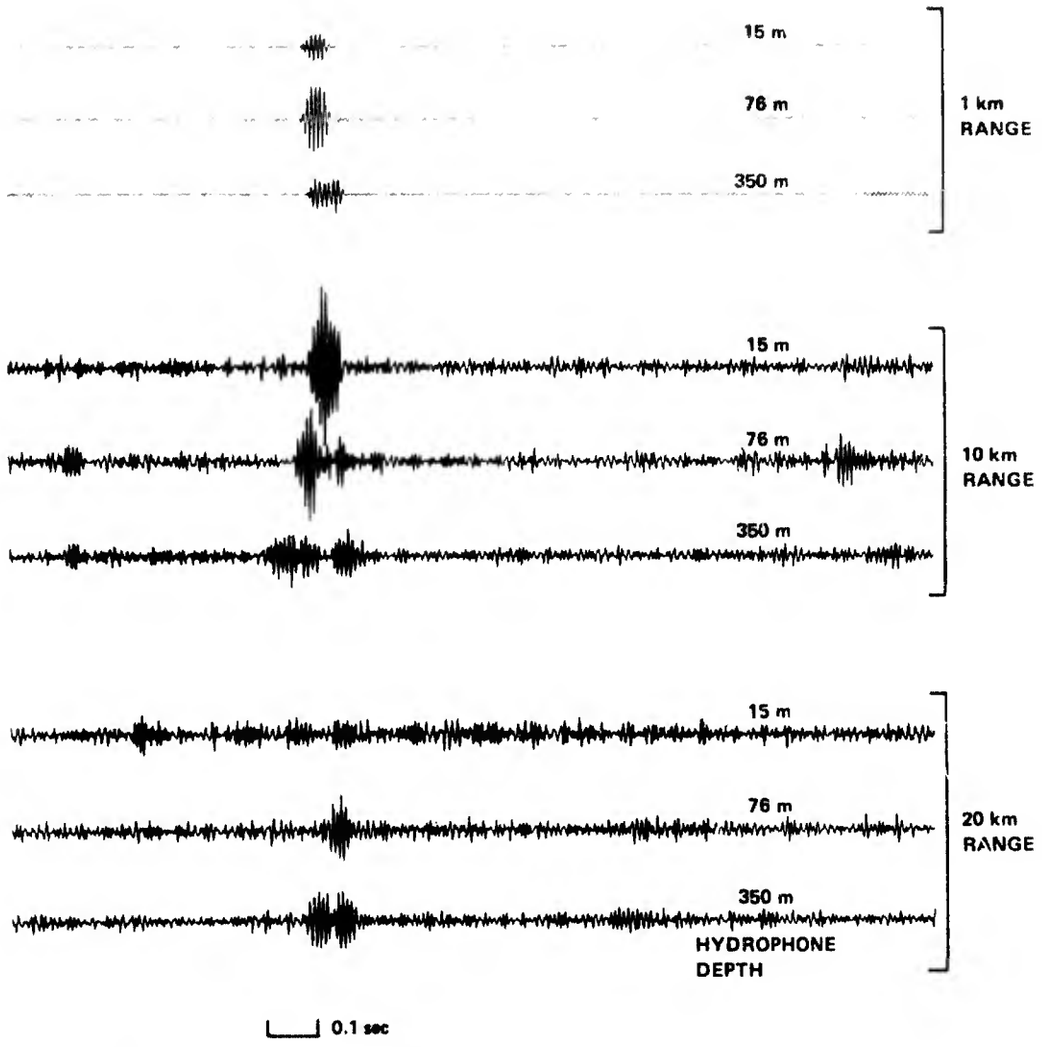

NOTE: GAIN SETTING FOR 1 km RANGE IS −13 dB WITH RESPECT TO SETTING FOR 10 AND 20 km RANGES.

Figure 13. Received Signal Time Structure at Several Ranges

A comparison of the total energy and peak value data does indeed show a progressively higher peak propagation loss with increase in range for all hydrophones as expected.

In addition to this, however, a second effect is also present. The total energy propagation loss determinations show, particularly beyond about 15 km, a significantly greater spread in values than the equivalent peak level figures. This appears unavoidable, and is most probably due to the subtraction of noise over the four-second sample period on the basis of a noise sample over the last 120 msec of each four-second period. Some of the spread may simply be statistical, and possibly would have been reduced if it were possible to take a longer noise sample. At the longer ranges, it is even possible that occasional stray signal arrivals were included in the noise sample period.

Since in this study we are most concerned with prediction of the multipath interference structure, we shall limit ourselves to discussion of those peak value propagation loss determinations which display this structure more clearly. Throughout this discussion, we must remain mindful of the inherent differences between pulsed and infinite CW propagation. Even if these differences may be overcome by resorting to pulse propagation modeling, it is often our ultimate goal to use the model to predict the propagation loss of essentially infinite CW signals from shipping. For this purpose, the fluctuations of the CW predictions may be more appropriate than the smoother fluctuations observed during experiments using transient signals.

RANGE-INDEPENDENT CW MODEL COMPARISONS

The first model considered is the Fast Field Program (FFP) for which a range-independent environment is assumed. Figure 14 shows propagation loss predictions for a source at 250 ft (76 m) and receivers at 350 (107 m), 750 (229 m) and 1150 ft (350 m), assuming a moderately low-loss bottom. At first glance, the correspondence of predictions with data appears quite good. There are, however, some significant differences in detail.

Close agreement with the structure of the 1150 ft (350 m) data is evident out to 9 kyd (8.2 km), although the model predicts a signal 3 dB stronger than that detected from 3 to 9 kyd (2.7 to 8.2 km). From 9 to 40 kyd (8.2 to 36.6 km) the model shows consistently stronger structure than is present in the data. Occasional peaks are predicted as much as 10 dB above the relatively smooth data, but correspondence of mean levels is reasonable. Much the same situation applies for the 750 ft (229 m) receiver, except that in the range 35 (32 km) to 40 kyd (36.6 km), the predictions systematically fall below measurement by as much as 8 dB.

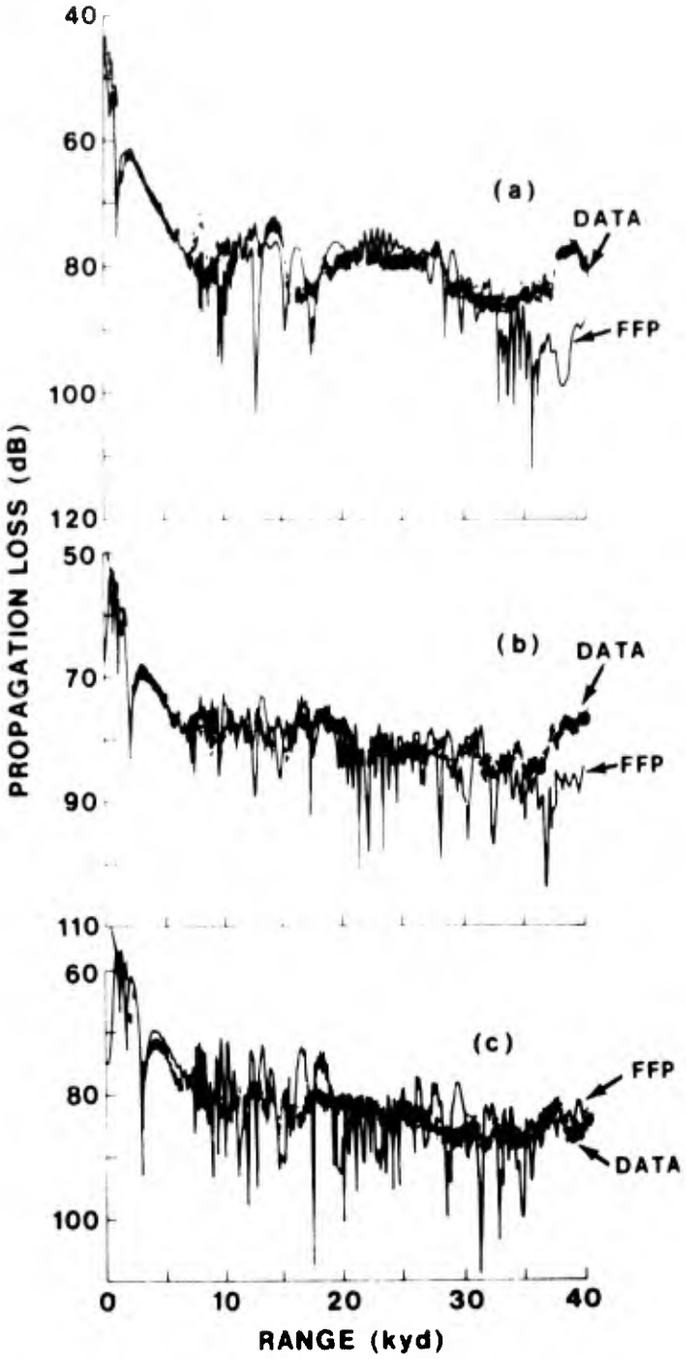

Figure 14. FFP Predictions, Source 76 m, Receiver Depth:
Curve (a) 107 m
Curve (b) 229 m
Curve (c) 350 m

Features which are present but not obvious in the deep cases become much clearer in the 350 ft (107 m) case, and for this reason in the remainder of this report we shall generally confine ourselves to the 350 ft (107 m) data for model comparisons. The 350 ft (107 m) experimental data show quite pronounced structuring, particularly in the form of broad peaks in the region 7 (6.4 km) to 15 kyd (13.7 km). A sudden drop in level at 15 kyd (13.7 km) precedes smaller scale features with a most notable increase between 37 (33.8 km) and 40 kyd (36.6 km), corresponding to a similar rise in the 750 ft (229 m) data. Turning now to the 350 ft (107 m) model predictions, the direct path to shadow zone transition region corresponds almost perfectly, and the model shows a region with structure of similar periodicity and magnitude to that of the 7 (6.4 km) and 15 kyd (13.7 km) region of the data. However, the peaks do not correspond exactly in range. In the region 35 (32 km) to 40 kyd (36.6) km, as for the 750 ft (229 m) case, the predicted levels are up to 10 dB below observed levels. We shall not concern ourselves further with the differences beyond 35 kyd (32 km), for reasons which we next consider.

Minor differences are apparent between the sound-speed profiles at the three stations along the track. Figure 15 shows the effect of these differences on FFP predictions. On the basis of the FFP fit to the direct path region, we choose to work generally with the profile corresponding to station 3 (see table 2).

Table 2. Station 3 Sound-Speed Profile Extended to Maximum Depth of 1828.8 m (1000 fm)
(Profiles in the remainder of this report are derived from this profile by truncation at the appropriate bottom depth)

Depth (m)	Sound-Speed (m/sec)
0.00	1538.94
76.20	1540.42
108.46	1541.04
167.64	1533.58
204.77	1528.91
304.43	1523.15
350.52	1522.26
444.80	1520.45
899.95	1490.16
1030.45	1487.70
1828.80	1495.22

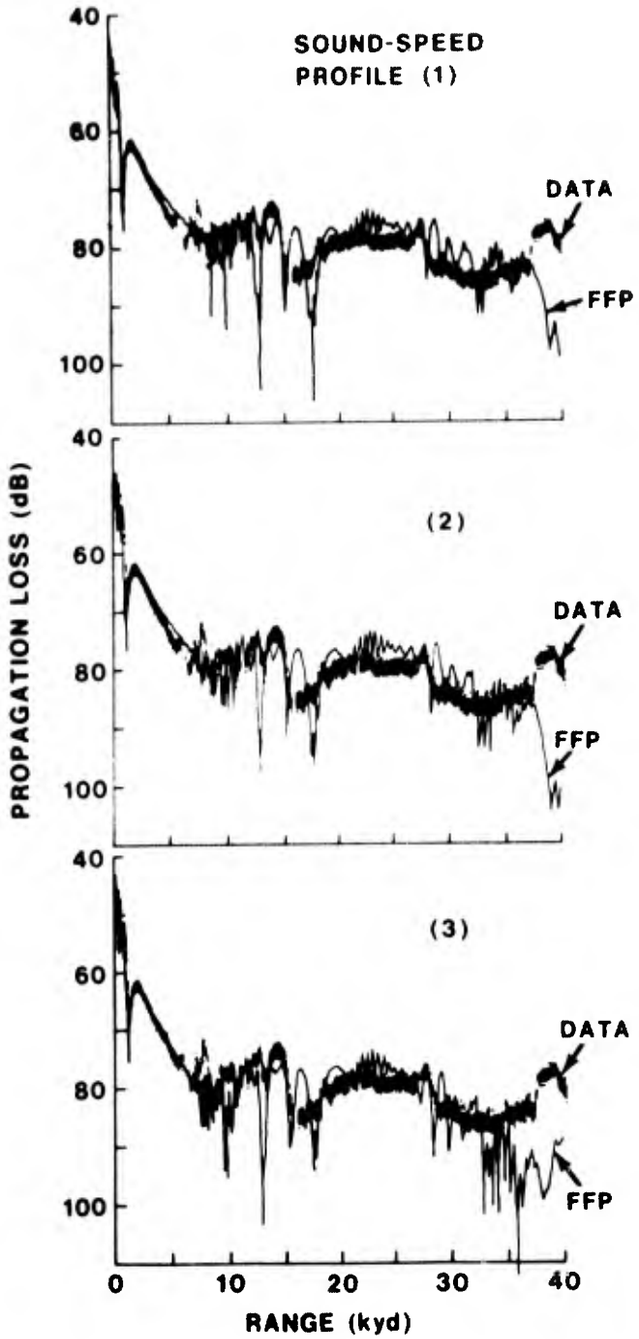

Figure 15. Direct-Path Region Fit of FFP to Experimental Data (Source 76 m, Receiver 107 m), Showing Effect Of Choice of Sound-Speed Profile

Only minor level changes between predictions with all three profiles are observed out to about 38 kyd (34.7 km). Beyond this range, cumulative phase differences, due to the small differences between the profiles, materially alter the interference structure of the prediction curve. At shorter ranges in the bottom bounce region, the choice of which profile to use does not appear to be critical.

Figures 16 and 17 show the effects of small perturbations to receiver depth and layer depth, modeled with the NISSM II program (reference 2). The predictions are demonstrably insensitive to small variations in these parameters. Small spatial or temporal variations in the medium, or variations in receiver depth cannot be cited, therefore, as the cause of imperfect agreement between data and model. It should be noted that quite close agreement in the structure of the coherent multipath interference pattern is evident between the NISSM II and FFP predictions for ranges greater than about 5 kyd (4.6 km).

The upper portion of figure 18 first compares the infinite CW CONGRATS predictions with the FFP, demonstrating excellent structural agreement beyond the Lloyd's mirror region. The difference in rate of shadow zone fall-off illustrates the influence of particular methods of sound-speed profile interpolation. Although nominally the same sound-speed profile data points are used for CONGRATS as for the FFP, in the CONGRATS case, interpolation is by means of a continuous curve fitting routine, whereas the FFP interpolation fits the profile by segments of exponential curves which closely approximate straight lines. That the shadow zone fall-off rate is a particularly sensitive indicator of profile shape is clearly demonstrated by the close structural agreement of the two predictions at greater ranges, showing that the profile fit has only a minor effect on multipath phase differences. The differences in level at long range are consistent with the differences in assumed bottom loss. The CONGRATS prediction assumes no bottom loss, whereas the FFP prediction is based upon the bottom loss shown in figure 19. For the profile given, the horizontal ray at the source has a grazing angle of 13.9° at the bottom, and the 25° source angle ray has a bottom grazing angle of 28.4°; hence, computed bottom loss will vary from less than 1 dB per bounce for the 14° grazing angle energy to about 4 dB per bounce for the 28° grazing angle energy. The bottom loss curve of figure 19 is based upon an infinite half-space bottom velocity of 1541/m/sec, and has been chosen simply on the basis of the fit of the FFP predictions to the data. It should be emphasized that this curve is not based upon any in situ measurement of bottom velocity at the measurement site, and that only the mean levels of bottom loss over the 14° to 28° region of the curve are significant in this example. Although some work on a variety of bottom-loss types, including some associated with

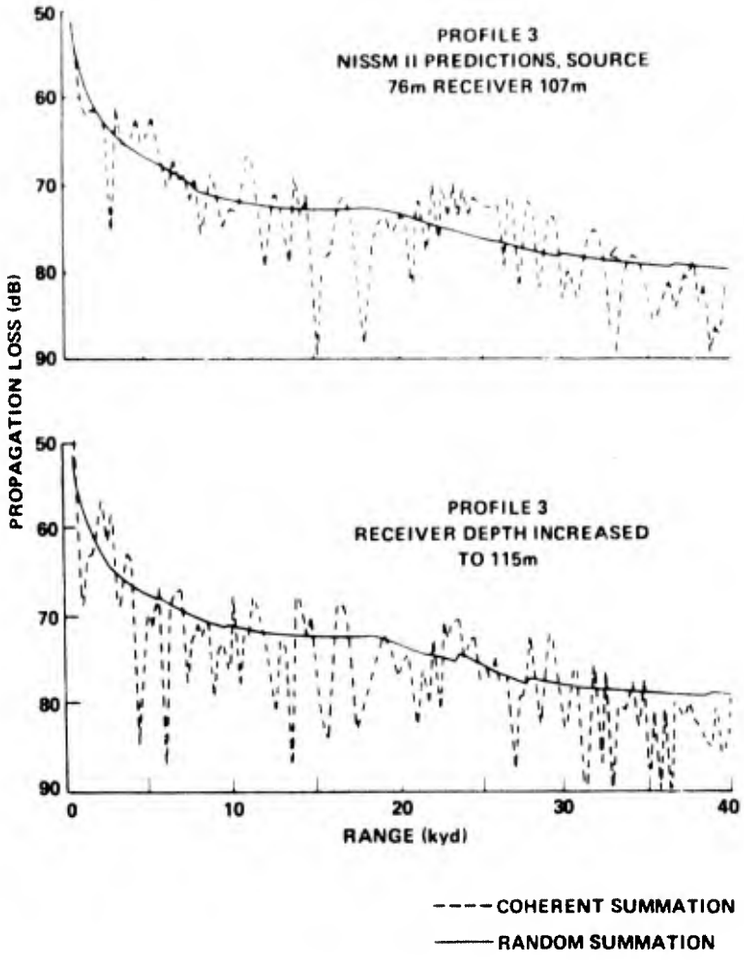

Figure 16. Perturbations to Input Parameters Establish Sensitivity Of Model Predictions to Small Errors in Placement of Receivers

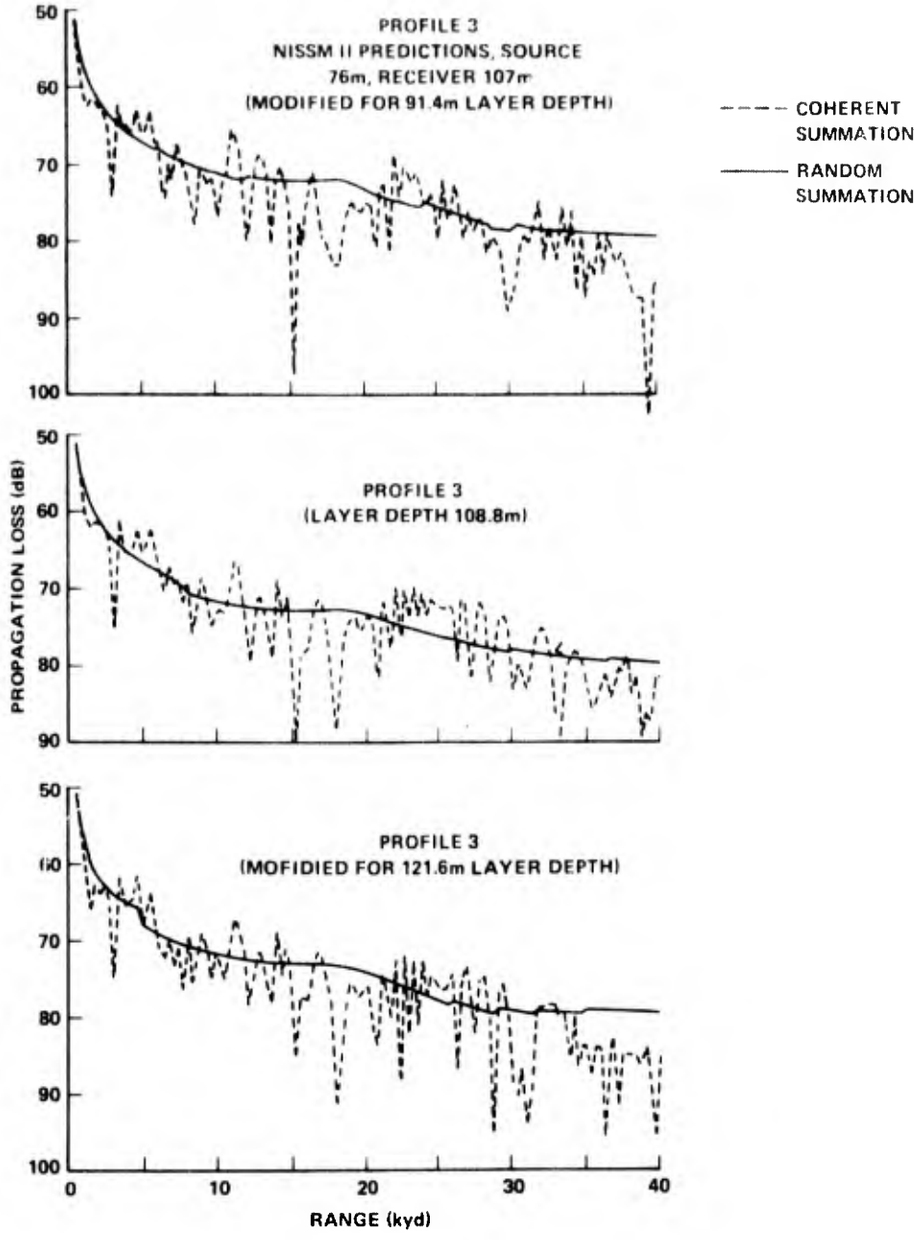

Figure 17. Perturbations to Input Parameters Establish Sensitivity of Model Predictions to Small-Range Or Time-Dependent Variations of Model Geometry

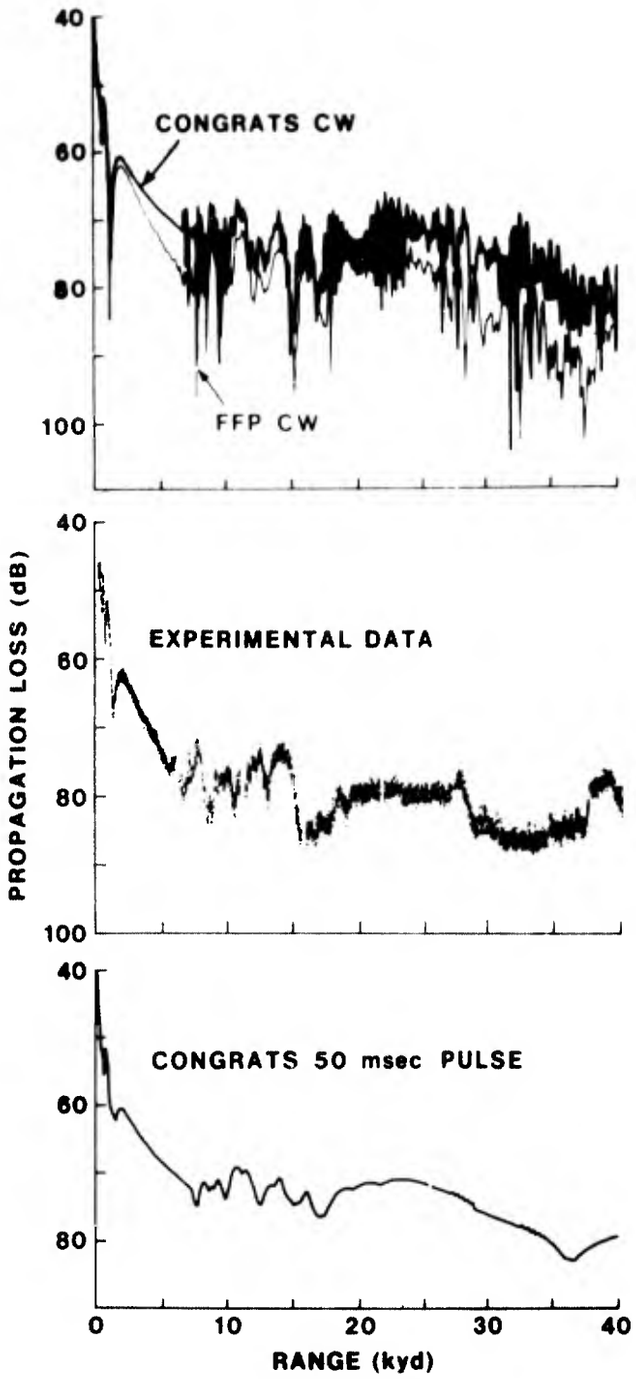

Figure 18. Effect of Finite Pulse Length on Multipath Interference Structure (Source 76 m, Receiver 107 m)

multilayer bottoms, was conducted in the early stages of this investigation, it soon became apparent that the influence of other factors, such as range dependence and finite pulse length, required resolution before it would be fruitful to proceed with any analysis of the effects of more complicated subbottom structuring. In general, therefore, throughout the following discussions, models have assumed either a low bottom loss or, where possible, zero bottom loss.

EFFECT OF FINITE PULSE LENGTH

So far, the models have assumed an infinite CW signal form, whereas the experiment involved 50 msec pulses. Multipath travel time differences will introduce variations into the degree of overlap of the various pulse arrivals, with a resultant modification of the multipath interference effects. The bottom curve of figure 18 is the CONGRATS prediction for a 50 msec pulse, peak arrival. Above it, for comparison, the experimental data are displayed again.

Both experiment and pulse prediction show direct path regions, then a region with four major interference maxima spaced about 2.5 kyd (2.3 km) apart, and generally beyond 30 kyd (18.3 km), a region with much less variation. It is clear that the curve more closely resembles the data than the rapid and pronounced fluctuations, even at long ranges, of the CW predictions.

Between 8 and 18 kyd (7.3 and 16.5 km), the CONGRATS pulse interference maxima line up with those of the CW predictions, not with those in the data; hence, the shift is not attributable to the differences between infinite CW and pulsed CW multipath interference effects. Another implication is that in the present case we may deduce at least some of the structure of the pulsed experimental data from consideration of even an infinite CW model.

So far, the ability of the modeling to reproduce major structural features of the data, although shifted in range, suggests that remaining differences are due to systematic differences between model and data, and may be resolved if these differences can be taken into account.

BOTTOM MODELING

PHASE PATH GEOMETRY

Two essential differences between model and experiment remain. These are source motion and bottom topography.

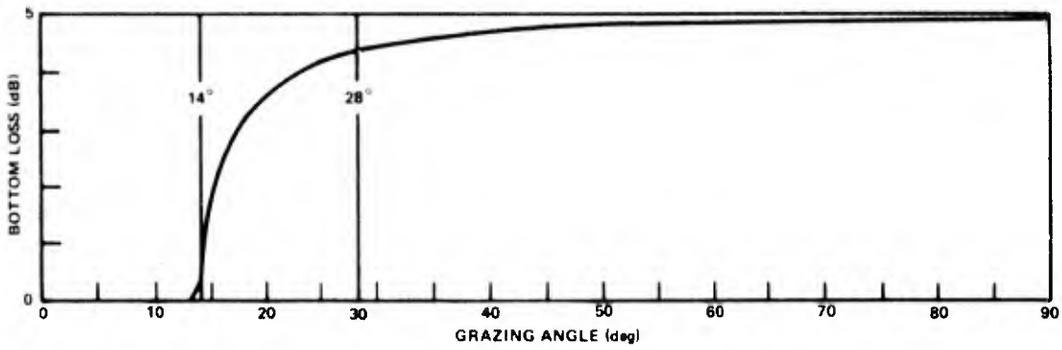

Figure 19. Bottom Loss Model Used for FFP Predictions

At only two knots with most significant multipath arrivals lying well within four seconds of each other, phase errors of generally much less than $\pi/2$ radians are introduced in coherent addition modeling if source motion is ignored, and the interference maxima will therefore be largely unaffected.

The actual bottom has a mean slope of half a degree. Over 40 kyd (36.6 km) this amounts to a change from 1800 to 1500 m in depth.

Figure 20 generated by the CONGRATS (reference 4) ray-tracing program demonstrates that the sloping bottom will compress the sound field slightly compared with the flat bottom case. More significant, however, is the obvious phase path difference, of the order of 200 π radians in 40 kyd (36.6 km) for the 25° source angle ray.

KANABIS SHALLOW WATER MODEL

The Kanabis shallow water model, a range-dependent normal mode program, was run for both a range-independent and a range-dependent bottom. The purpose was both to test the model against the data, and to note any systematic differences between the range-dependent and the range-independent predictions. Predictions based upon the sum of modes 37 to 84 are shown in figure 21. It should be noted, that, because of the large percentage change in depth over the range involved, the proper consideration of the model constraints dictates a division of the range into perhaps a dozen or more shorter segments, within each of which the percentage change in bottom depth is much less appreciable. However, because of the large number of modes involved, this course of action would make heavy demands upon computer time. The model was never intended for the water depths present in this case, but is particularly interesting in that it takes partial account of the conversion of energy from one mode to another in response to changes in water depth, in addition to the adiabatic changes more commonly employed in normal mode models. As a compromise, the range was divided into three segments for the range-dependent predictions, and comparison with the range-independent predictions shows a tendency, particularly beyond 20 kyd (18.3 km) for the range dependence to increase the loss by about 5 dB, and to provide a generally better fit to the data.

Two cautionary notes should be sounded here. The first is that the flat bottom FFP predictions already discussed lie much closer to the level of the data than the flat bottom, shallow water model predictions. The difference between the FFP and shallow water model, flat bottom predictions has a simple explanation. The FFP case was run assuming a small bottom loss,

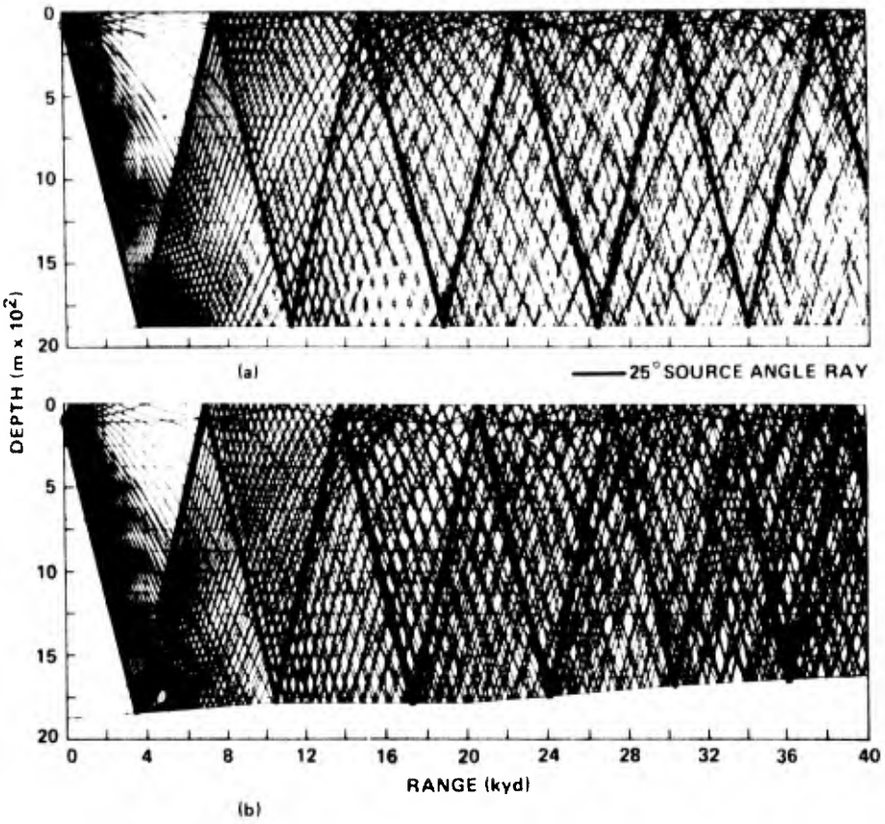

Figure 20. Ray Diagrams Comparing Sound Field.

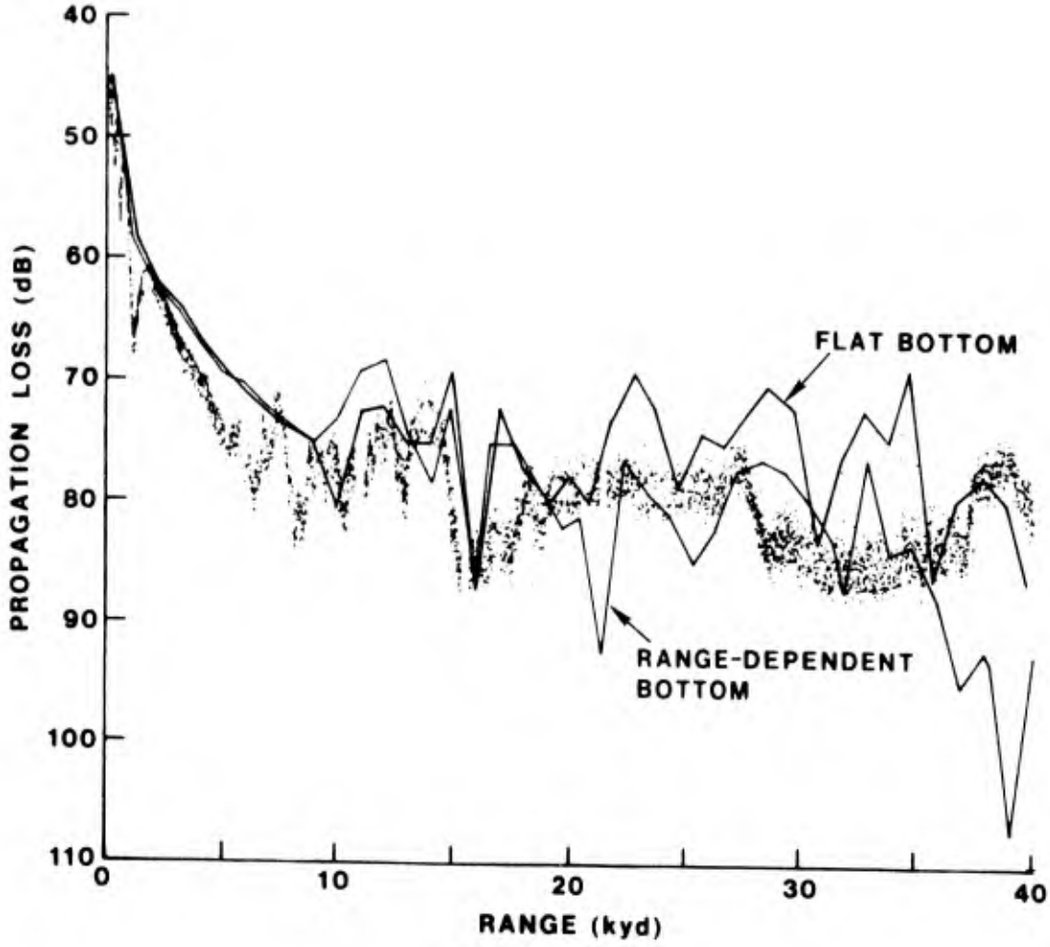

Figure 21. Range-Dependent Normal Mode (Kanabis Model) With Partial Mode Conversion (Source 76 m, Receiver 107 m)

whereas no bottom loss was assumed for the propagating modes of the shallow water model in this instance. The bottom loss in the FFP case was chosen to give the best mean fit to the data. However, if the additional loss due to bottom slope predicted by the shallow-water model in this case is a real effect, then the shallow water model predictions indicate that the zero bottom-loss figure is the more appropriate. The second cautionary note is that in the present predictions, the data points for the shallow water model are approximately 1 km apart, and comparison with the FFP predictions shows that at this spacing the fine structure of the coherent multipath interference pattern is being undersampled. When this is combined with a linear interpolation on a logarithmic scale, which might be an acceptable device at a much higher sample density, a quick glance at the predictions may give a misleading impression, unless the reader is cognizant of the reasons for the predictions being as they are.

Within the limitations as expressed, the predictions of the shallow water model may be regarded as quite acceptable. They have been included for the sake of completeness, and because they serve to illustrate some of the difficulties which may be encountered in the application of a model to a particular problem outside its intended design limits. Our defense of this unfair treatment of the model is that it is the only available mode model which attempts to deal with nonadiabatic mode coupling, and for this reason is particularly interesting. Primarily because of the undersampling, it would not be constructive to examine in detail the significance of the individual peaks in the prediction.

THREE-DIMENSIONAL BOTTOM TOPOGRAPHY

The horizontal ray (or 3-dimensional normal mode) program (reference 6) was kindly made available by Dr. Weinberg of NUSC, although still a developmental rather than a production program.

It was first run for the flat bottom case, using 130 modes. As shown in figure 22, agreement with the FFP was almost perfect. It agreed even more closely than the FFP with the initial bottom bounce arrival prediction, since the FFP was limited to $\pm 25°$ at the source, whereas the higher modes used correspond roughly to $\pm 35°$ source angles. The third curve shows the FFP collapsed one more time, thus representing source angles up to $\pm 49°$, with the expected results.

Since the cruise track was above a shallow depression in the ocean bottom, bottom reflections slightly off vertical might conceivably still provide paths between source and receiver. This was tested in apparently the first use of the

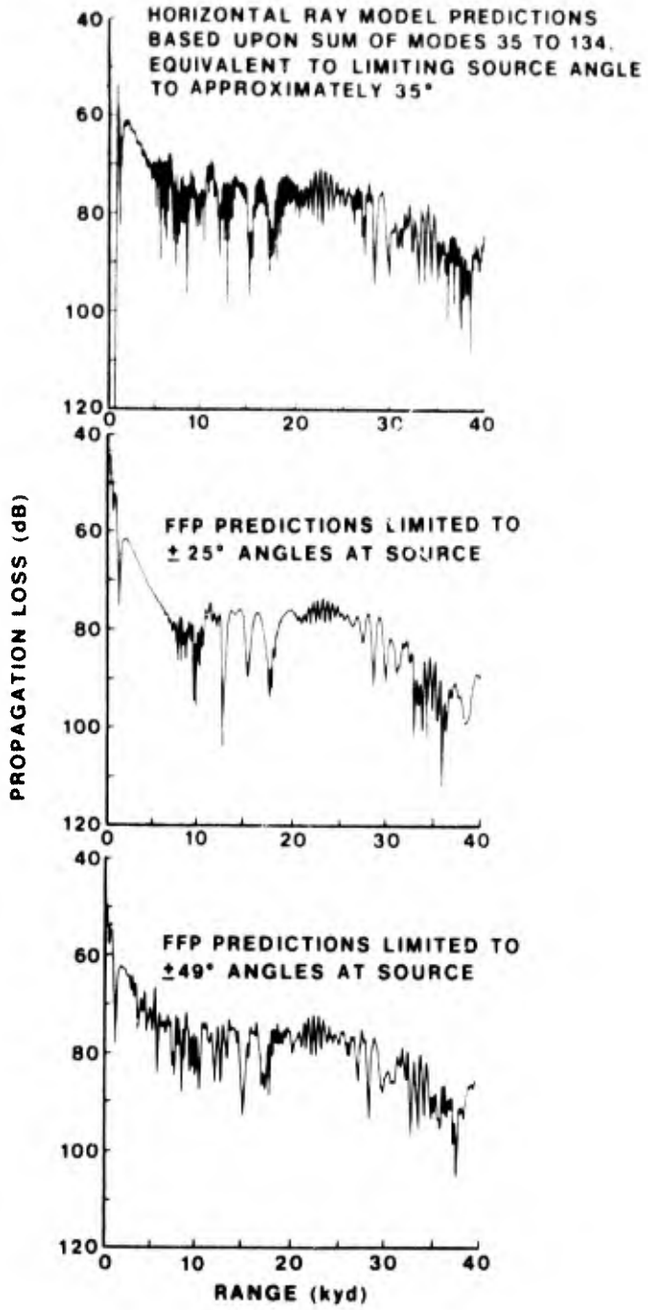

Figure 22. Comparison of Horizontal Ray Theory and FFP Predictions For a Range-Independent Case (Source 76 m, Receiver 107 m)

horizontal ray program with actual three-dimensional data. Three-dimensional bottom variation was input to the program as a 5 x 3 grid of bottom depths: 5 points spaced along the track 10 kyd (9.1 km) apart, and each of these points being the center point of 3 points across the track 2 kyd (1.8 km) apart, making a total of 15 bottom points on a 5 x 3 grid. Resulting transmission loss predictions are shown in figure 23.

A comparison with predictions constrained to the plane of the cruise track only, represented as a 5 x 1 grid of points, yields almost the identical interference structure.

In the 5 x 3 case, however, there is a slight compression of the pattern consistent with some horizontal curvature of the propagation paths. The interference structure is determined by the arc of the curve, whereas the range is equivalent to the chord. At 40 kyd (36.6 km) the shift amounts to about 1 kyd (0.9 km).

Both predictions show reasonable mean level agreement with the data, but differ distinctly in structure. In some sections, they almost appear to be in antiphase to the data.

On the assumption that the 5-point representation of the bottom may have strained the "slow variation" constraint and thus program accuracy, or that modeling the bottom too coarsely may have introduced gross errors into the phase paths, the bottom was modeled finally by a 16-point linear grid. This changed the direct path region a little, showing the presence of bottom reflected energy even at about 4 km, but otherwise left the structure almost completely unaltered, demonstrating that the program was handling the 5-point step change adequately, and that 5-point modeling was adequate to represent most of the important features contributing to the phase paths. No doubt, errors partially cancel.

SUBBOTTOM MODELING

Predictions have also been made with a Canadian version of the parabolic equation model (reference 7) and a version now in use at the Naval Underwater Systems Center (reference 8).

The parabolic equation method (reference 10) provides a flexible technique for modeling range dependence. However, it does suffer practical operating difficulties, particularly when trying to represent a water column to bottom

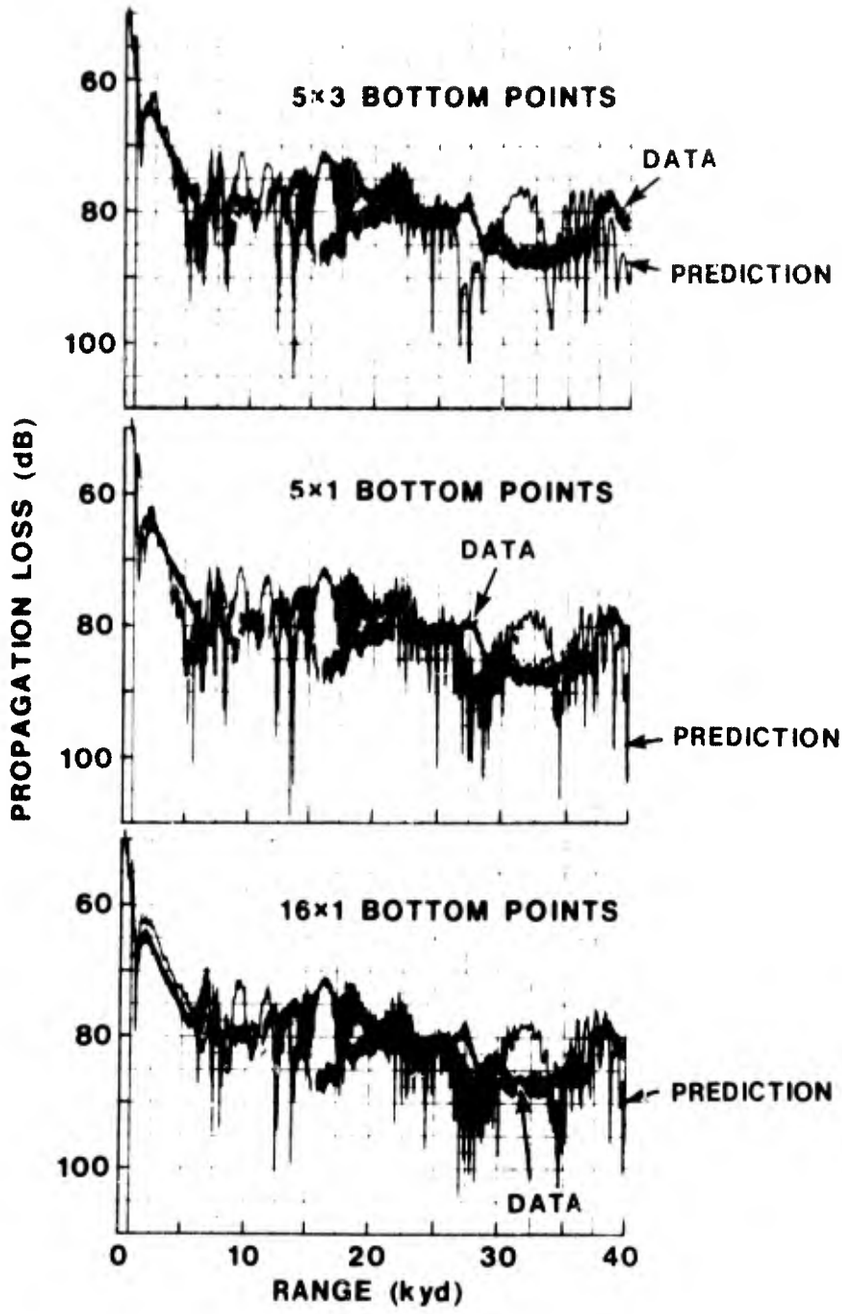

Figure 23. Comparison of Horizontal Ray Theory (3-Dimensional Mode) With Experimental Data, Assuming Range-Dependent Bottom (Source 76 m, Receiver 107 m)

sound-speed discontinuity, which it must approximate by a continuous profile. The difficulty arises from the need to keep errors introduced into the marching solution small so that they do not grow in range to the point where they render the predictions at greater ranges of interest meaningless. In practice, this may be achieved only if the range increment in the solution bears an inverse relationship to the magnitude of the maximum sound-speed profile gradient. This means that the sharper the increase in sound speed from water column to bottom, the shorter the allowable range step is, and the larger the number of calculations involved in predicting propagation loss to any given range. Since for every range step, the model must carry out two fast Fourier transforms (FFT), in most practical problems computing time dictates a conscious effort to minimize the number of range steps necessary. If hardware FFT processors are available instead of the more generally available software routines, increases in calculation speed of the order of one thousand times may be attainable, in which case some of the present limitations to the practical application of the parabolic equation technique may be greatly revised.

We first consider predictions with the Canadian version. The upper sound-speed profile of figure 24 models a semi-infinite isovelocity bottom. The bending of the intensity bands across the bottom interface region apparently follows Snell's law. This is logical, when we bear in mind that the bands of high intensity may be regarded as regions in which multipath rays add constructively. Since the rays follow Snell's law in the vertical direction, the intensity bands will tend to reflect this behavior. Beyond critical angle, a reflection or, possibly in this instance, a refraction of energy back into the water is evident.

In the lower case, a hard bottom is simulated by extending the 1 m/sec/m increase in sound speed indefinitely into the bottom, so that ultimately all energy will be refracted. Figure 25 shows that for both the flat-bottom and range-dependent cases, predicted levels for the hard bottom (curve (b)) are close to those for the data, whereas the isovelocity bottom predictions of curve (a) are mostly much too low.

Possibly the most interesting feature of the predictions is the range discrepancy between the first interacting bottom arrivals and those of the data. The physically realistic refraction of the model is insufficient to match the two. The difference confirms that reflection rather than refraction is the more probable bottom mechanism in this instance, consistent with a hard, coralline limestone only thinly overlain by sediments. Since all distant paths in the predictions of curve (b) include subbottom refraction, it is not surprising that there is no fine-scale agreement with the FFP and other hard bottom models, nor with the experimental data.

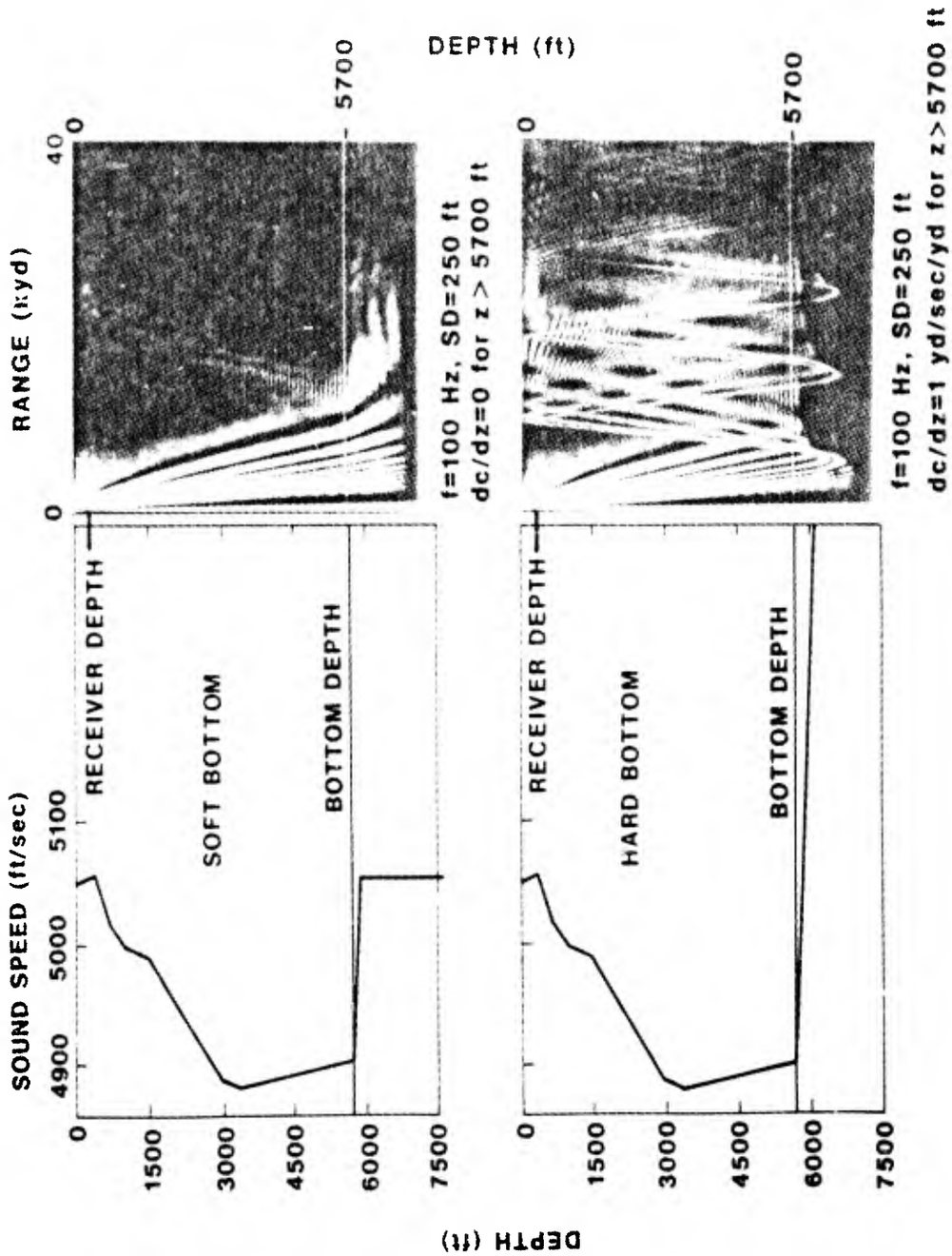

Figure 24. Parabolic Equation (Canadian) Range-Depth Propagation Loss Diagrams (Intensity Scale: White $\leq$ 60 dB; Black $\geq$ 100 dB)

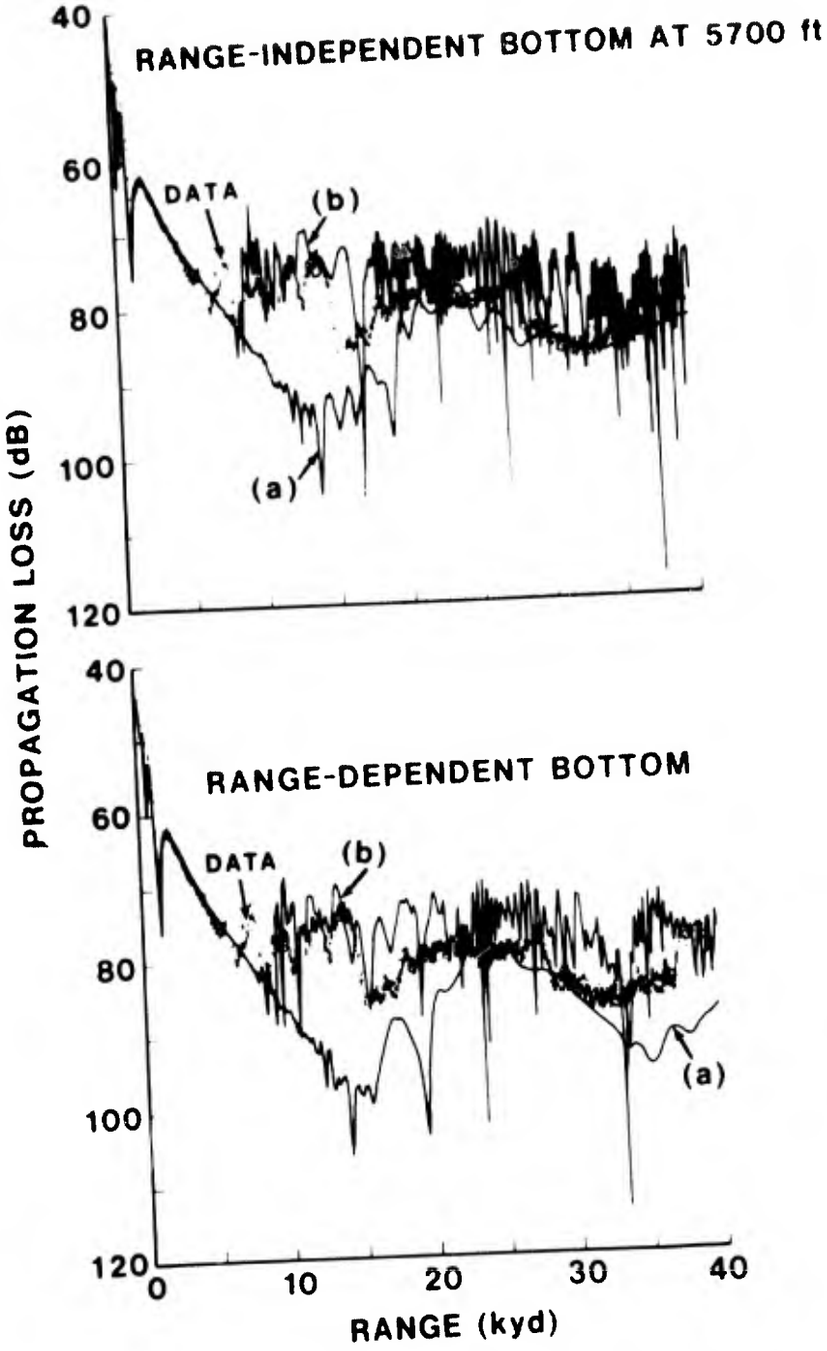

Figure 25. Parabolic Equation (Canadian) Predictions Compared With Experimental Data (Source 76 m, Receiver 107 m)

Curve (a) Semi-infinite, Isovelocity Bottom
Curve (b) Hard Bottom

Turning now to the NUSC parabolic equation model, we first study the bottom refraction modeling one step further. Figure 26 shows the PE predictions for a subbottom gradient of 1 m/sec/m, based upon a starting field of 100 modes. The generally high values of propagation loss for the bottom interacting energy is attributable to the assumed bottom absorption of 0.1 dB per wavelength. Increasing the bottom gradient to 4 m/sec/m and reducing the absorption to 0.01 dB per wavelength produces the predictions of figure 27. Interestingly, some of the features of the previous predictions are recognizable again in this case, although laterally shifted and showing less loss. Even more interesting, though, is the comparison with the original FFP predictions which actually modeled a sharp bottom discontinuity. Out to a range of 30 kyd (27.4 km), there is exceptionally close agreement between the PE and FFP predictions in the structure of the curve and the range of the major features, indicating that the 4 m/sec/m subbottom gradient is sufficient in this instance to model the hard bottom interface. The lower propagation loss levels for the PE are consistent with the differences in assumed bottom loss between the two models and, as has already been discussed for the FFP, the inclusion of additional modes in the starting field calculations for the PE would no doubt inject more energy into the region around 7 kyd (6.4 km).

Finally, a range-dependent prediction was made with the NUSC PE model, representing the bottom by twelve separate segments. The results are shown in figure 28. With the high bottom gradient, the bottom absorption of 0.01 dB per wavelength represents almost zero bottom loss, and comparison of the mean level with the data indicates that a slightly larger bottom loss might be more appropriate. As for detailed agreement in range with the major features of the data, though, the 12-segment range-dependent prediction seems no closer to a good match than the flat bottom prediction. To a limited extent, some lateral shifts to the prediction peaks may be effected by local variation of segment depths, but in the light of the detailed knowledge of bottom topography in the present case, this excuse is denied us. The NUSC parabolic equation model represents the bottom by a series of constant depth segments, rather than true slopes, and so possibly modeling the bottom by only twelve segments is still inadequate.

AN OBSTACLE TO RANGE-DEPENDENT PULSE MODELING

So far we have only touched on the pulse modeling problem. By running the CW FFP for a range of frequencies, we are able to determine pulse propagation loss by Fourier transform techniques. Curve (b) of figure 29 shows FFP 50 msec pulse predictions for the 1150 ft (350 m) receiver depth case, and curve (c) shows CONGRATS predictions for comparison.

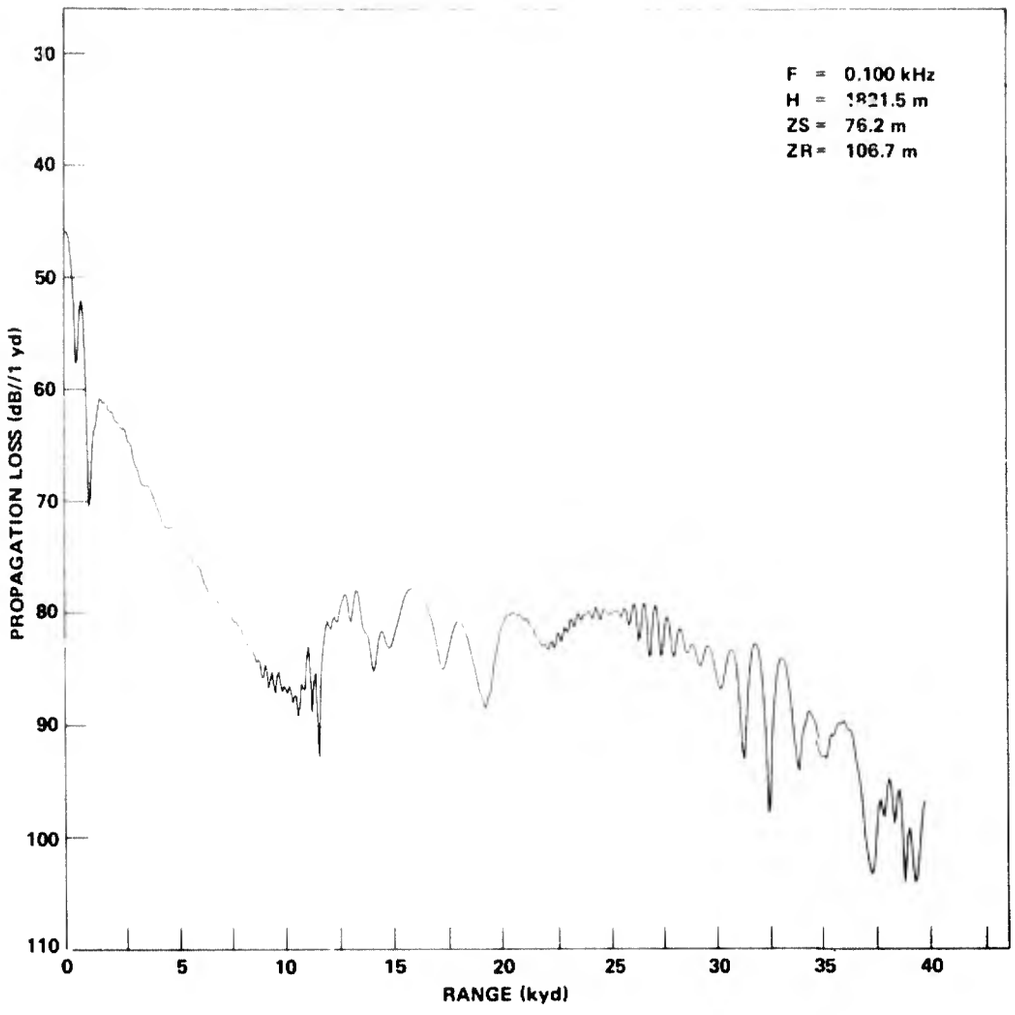

Figure 26. NUSC Parabolic Equation Model Predictions for Range-Independent Case (1 m/sec/m Sound-Speed Gradient In Bottom, 0.1 dB/λ Bottom Attenuation)

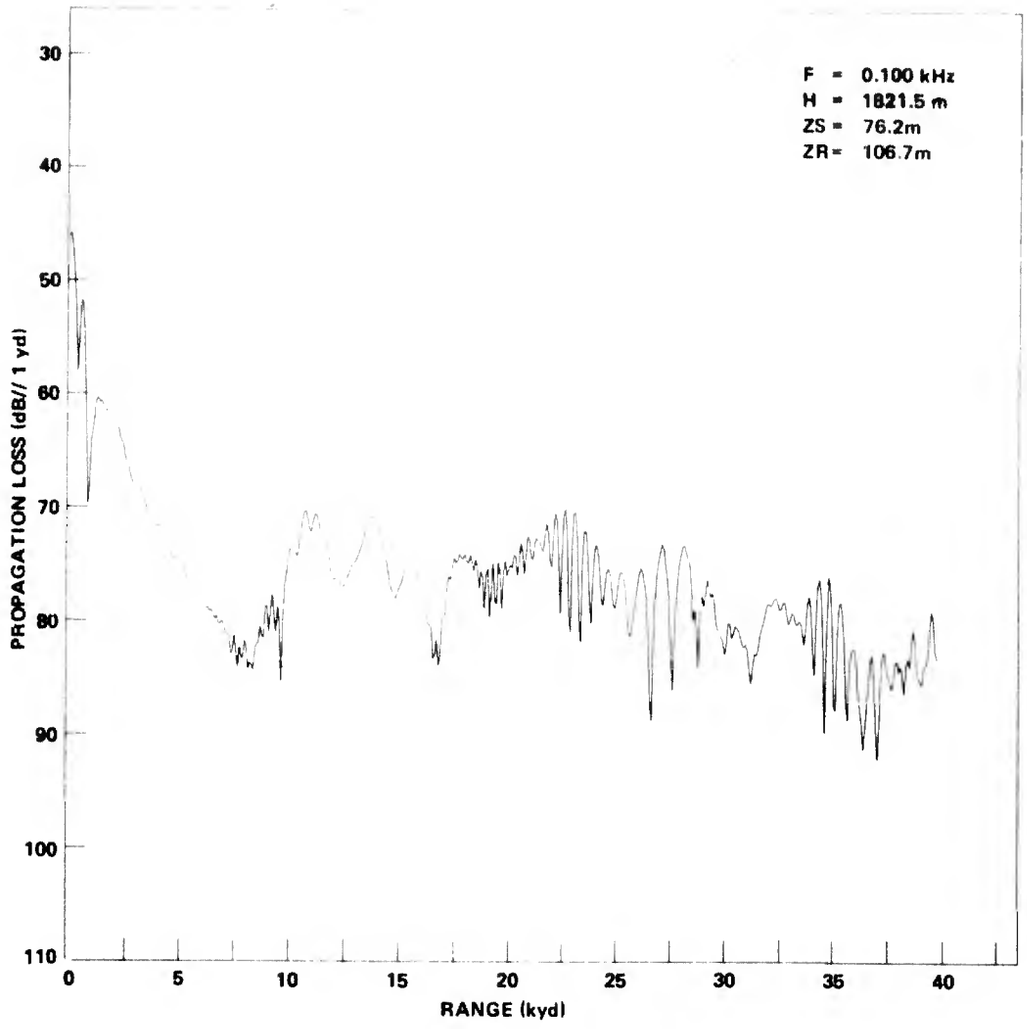

Figure 27. NUSC Parabolic Equation Model Predictions for Range-Independent Case (4 m/sec/m Sound-Speed Gradient In Bottom, 0.01 dB/λ Bottom Attenuation)

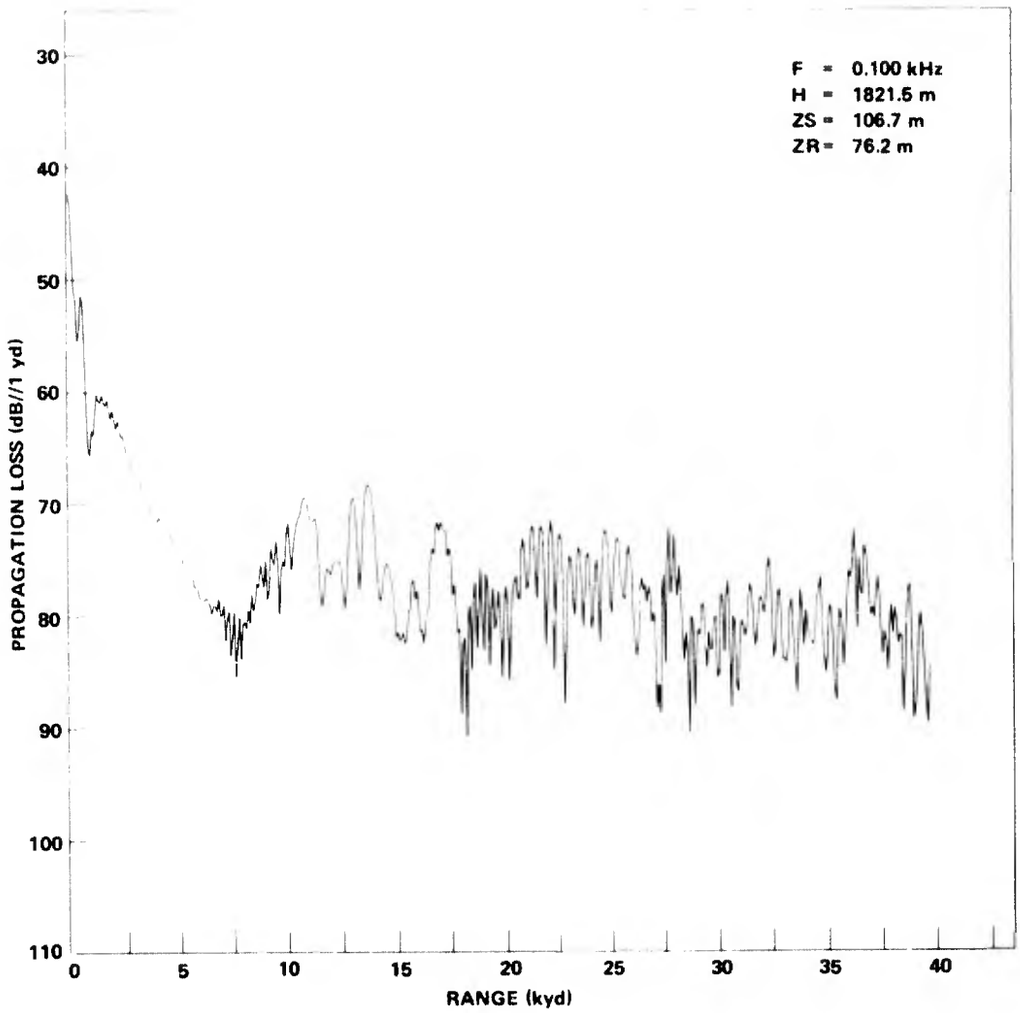

Figure 28. NUSC Parabolic Equation Model Predictions for 12-Segment Range-Dependent Bottom, Otherwise Conditions Are As In Figure 27

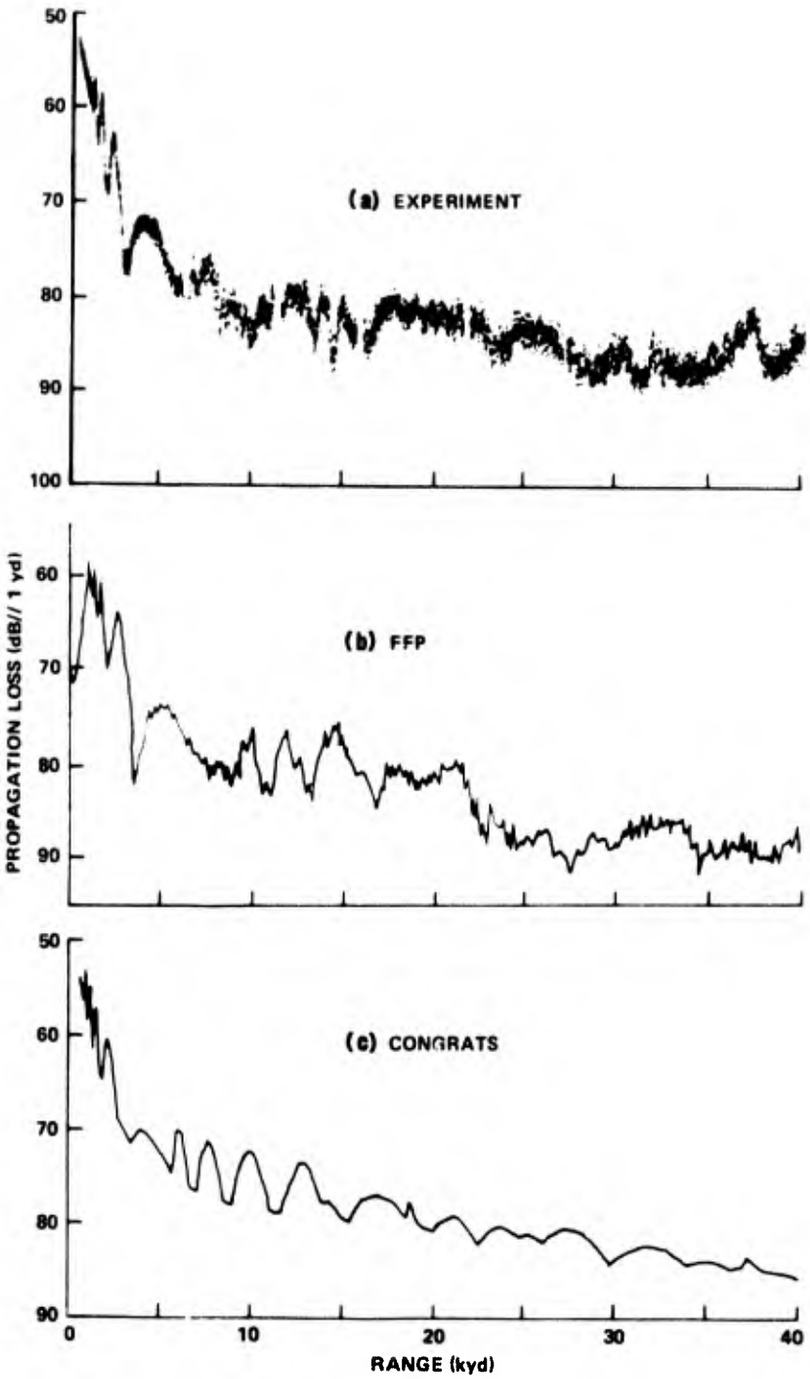

Figure 29. Comparison of FFP Fourier Synthesis Pulse Propagation Loss Modeling With CONGRATS Ray Theory Model and Experimental Data (50 msec Pulse, Receiver Depth 350 m)

Theoretically, there should be no reason why the FFP Fourier synthesis could not be applied to coherent predictions from the parabolic equation or to any other full-wave model, to bring pulse and range dependence into the one prediction. We can generally expect a single CW range-dependent prediction run in such a case to require much more than the 4 minutes of computer time needed in this case by the CW FFP, possibly even by a factor of ten or more. When we multiply that fact by the knowledge that the single pulse curve (b) represents 30 hours of computing with the FFP, then the range-dependent pulse possibility seems more like something that must await a new generation of computers. We would need good reason to tie up a computer for a month or more on one propagation loss prediction, particularly if our confidence in the answers obtained were less than absolute.

CONCLUSIONS

In conclusion, let us not forget that the task we have set the models is one of the hardest they could face, and that they have generally come through well. Obvious similarities between experiment and model in terms of level fluctuations and in terms of mean levels have been demonstrated. Different circumstances would generally favor one model rather than another, and wise choice of the most appropriate model would then be expected to give excellent agreement.

No single model has been able to replicate the data. Together, however, the models tell us much about the relative importance of the various environmental parameters. As might be expected, bottom topography and subbottom structure have a key role in the present case. The need for a thorough understanding of the bottom reflection-refraction process is clearly demonstrated.

Even assuming that adequate subbottom modeling combined with a range-dependent pulse model would enable model replication of the major features of the experimental data, the dependence on detailed knowledge of environmental data, and on accurate navigation, casts doubts on the applicability of such modeling to more generally realizable situations.

One of the problems incidental to this study has been the difficulty of properly comparing CW model predictions with pulsed experimental data. Quite irrespective of the influence of range-dependent bottom topography, our study has been limited in the area of pulse modeling simply by the cost of computer time. This highlights a potentially serious situation with impact far more general than the present study.

In order to optimize the performance of a new generation of sophisticated sonar processing systems, we must improve our understanding of the wavefront prediction problem. Practical understanding of the propagation of general transient signals can be verified and extended only by the use of suitable models.

The theory for flexible transient propagation loss modeling based on Fourier synthesis, using full-wave CW models, is well known, and its use has been demonstrated in this study. However, the modeler's ability to utilize this theory is limited drastically by the cost of computing time. Until faster, but still accurate, pulse modeling techniques can be developed, this major front for research and development effort will remain almost virgin territory.

LIST OF REFERENCES

1. F. R. DiNapoli, Fast Field Program for Multilayered Media, NUSC Technical Report 4103, 26 August 1971.

2. H. Weinberg, Navy Interim Surface Ship Model (NISSM) II, NUC Technical Publication 372 and NUSC Technical Report 4527, 14 November 1974.

3. J. S. Cohen and L. T. Einstein, Continuous Gradient Ray-Tracing System (CONGRATS) II: Eigenray Processing Programs, NUSL Report No. 1069, 5 February 1970.

4. H. Weinberg, CONGRATS I: Ray Plotting and Eigenray Generations, NUSL Report No. 1052, 30 October 1969.

5. W. G. Kanabis, A Shallow Water Acoustic Model for an Ocean Stratified in Range and Depth, Vol. I, NUSC Technical Report 4887-I, 25 March 1975.

6. H. Weinberg and R. Burridge, "Horizontal Ray Theory for Ocean Acoustics," Journal of the Acoustical Society of America, Vol. 55, 1974, pp. 63-79.

7. D. J. Thomson, Private Communication, 1975.

8. G. Gartrell, "Implementation of a Parabolic Equation Model on the NUSC UNIVAC 1108," NUSC Technical Memorandum TA11-232-76 (in preparation).

9. U. S. Naval Oceanographic Office, Environmental Atlas of the Tongue of the Ocean, Bahamas, Special Publication SP-94, 1967.

10. F. Tappert and R. Hardin, in C. W. Spofford, A Synopsis of the AESD Workshop of Acoustic Propagation Modelling by Non-Ray-Tracing Techniques, 22-25 May 1973, Washington, D. C., AESD Technical Note TN-73-05, November 1973.

INITIAL DISTRIBUTION LIST

Addressee	No. of Copies
CINCLANTFLT (1) (R. Chapman, Science Advisor (1))	2
CINCPACFLT	1
COMSECONDFLT	1
COMTHIRDFLT	1
COMSIXTHFLT	1
COMSEVENTHFLT	1
COMASWFORSIXTHFLT	1
COMSUBLANT	1
COMSUBPAC	1
COMSUBDEVGRUONE	1
COMSUBDEVGRUTWO (1) (CDR J. Dobes (1))	2
ASN (R&D)	1
ONR, Code 102-OS, 412-3, 480, 483, 485	5
CNO, OP-02, -03EG, -090, -095, -098, -098T, -201, -23T, -953, -954, -96, -96C, -96C1, -981G, -981H	15
CNM, MAT-00, -03B, -03L, -03L4, -03R, SP-20, ASW-14, -23, -24	9
DDR&E (G. Cann)	2
NRL	1
SUBASELANT	1
OCEANAV	1
NAVOCEANO, Code 02, 7200, 9320	3
NAVELECSYSCOMHQ, Code 03, PME-124	2
NAVSEA, SEA-03C, -032, -06H, -06H1, -06H1-4, -660C, -660F	7
NAVAIRDEVCEN	1
DTNSRDC	1
NAVCOASTSYSLAB	1
NELC	1
NUC	1
NISC	1
NAVSUBSCOL	1
NAVPGSCOL	1
APL/UW	1
ARL/PENN STATE, State College	1
DDC, Alexandria	12
Woods Hole Oceanographic Institution	1
U. S. Geological Survey (Dr. James Balsley, Assist. Director Land Resources, Reston, VA)	1
Naval Hydrographic Office, Avenida Montes De Oca 2124, Buenos Aires, Argentina (Dr. Jorge C. Novarini)	1
U. S. Navy Section, U. S. Military Group, Brazil (CDR Carlos Parente)	1